CRYSTAL GROWTH & DESIGN

pubs.acs.org/crystal

Article

Exploring "Triazole-Thiourea" Based Ligands for the Self-Assembly of Photoluminescent Hg(II) Coordination Compounds

Houria Benaissa, Nayarassery N. Adarsh, Koen Robeyns, Jakub J. Zakrzewski, Szymon Chorazy, James G. M. Hooper, Filip Sagan, Mariusz P. Mitoraj, Mariusz Wolff, Smaail Radi, and Yann Garcia*

Cite This: *Cryst. Growth Des.* 2021, 21, 3562−3581

Read Online

ACCESS | Metrics & More | Article Recommendations | Supporting Information

ABSTRACT: This study represents the first explorative investigation on the supramolecular structural diversity in Hg(II) coordination chemistry with triazole-thiourea ligands leading to a variety of mononuclear, binuclear, and coordination polymers: {[Hg(**L1**)$_2$(**L1**$^-$)$_2$]} (**1**), {[Hg$_2$(**L1**)$_2$(μ_2-I)$_2$I$_2$]·DMSO} (**2**), {[Hg(**L2**)(μ_2-I)I]·MeOH}$_\infty$ (**3**), {[Hg$_2$(μ-**L3**$^-$)$_4$]}$_\infty$ (**4**), {[HgCl(**L4**$^-$)**L4**]·MeOH} (**5**), {[Hg$_2$(**L4**)$_2$(μ_2-I)$_2$(I)$_2$]·2MeOH} (**6**), {[Hg$_2$(μ_2-**L5**$^-$)$_4$]}$_\infty$ (**7**), {[Hg$_2$(μ_2-Cl)$_2$(**L6**$^-$)$_2$(**L6**)$_2$]} (**8**), {[Hg$_2$(μ_2-Br)$_2$(**L6**$^-$)$_2$(**L6**)$_2$]} (**9**), and {[Hg$_2$(μ_2-I)$_2$(**L6**$^-$)$_2$(**L6**)$_2$]} (**10**). A reaction mechanism was suggested for the unexpected ligand rearrangement occurring in {[Hg$_2$I$_3$(μ_3-**L5**′)]}$_\infty$ (**11**). The ligands were fully characterized including by X-ray crystallography and computational means. This includes six new triazole-thiourea based ligands, namely, 1-R-3-(4*H*-1,2,4-triazol-4-yl)thiourea (where R = methyl (**L1**), ethyl (**L2**), propyl (**L3**), isopropyl (**L4**), and its polymorph (**L4-poly**), allyl (**L5**), ethyl acetate (**L6**), and its solvate (**L6_MeOH**)). Under UV light excitation, **7**, **10**, and **11** exhibit visible photoluminescence of wide origin, ranging from ligand-centered (LC) fluorescence combined with organic-ligand-to-metal charge transfer (LMCT) emissive states in **7** and **10**, up to halide-to-metal charge transfer (XMCT) combined with halide-to-ligand charge transfer (XLCT) emissive states in **11**. The variable emission mechanisms in the obtained coordination polymers were elucidated by experimental proofs confronted with theoretical calculations of the electronic densities of states, proving that Hg(II) halide coordination polymers involving flexible 1,2,4-triazole-based ligands form a promising class of luminescent molecular materials.

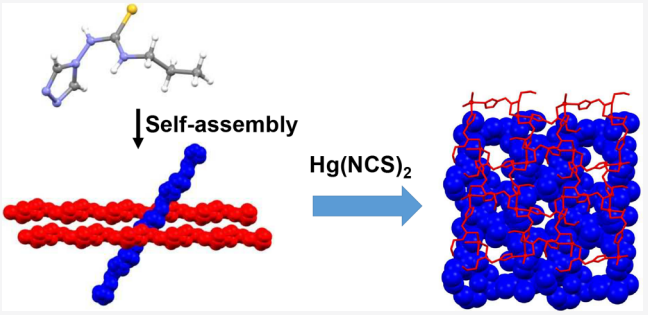

INTRODUCTION

The journey of 1,2,4-triazole chemistry started with the seminal work by Bladin in 1885.[1] Even though the synthesis of 1,2,4-triazole was established over a century ago, researchers are still working on the design and synthesis of new 1,2,4-triazole compounds,[2] due to for instance their antiviral, anti-inflammatory, antimicrobial, and anticancer properties.[3] The 1,2,4-triazole moieties present in these biologically active compounds justify the criteria for a potential active drug; for example, ribavirin, fluconazole, and rizatriptan are the drugs containing 1,2,4-triazole units for treating antiviral, antifungal, and antimigraine infections, respectively.[4] Inspired by the coordination ability of 1,2,4-triazole ligands to form various coordination network structures, many coordination and material chemists including us[5−10] developed interesting one- (1D), two- (2D), and three (3D)-dimensional coordination polymer (CP) architectures.[11−13] CPs have been recognized as intriguing porous materials[14,15] due to their fascinating structures, and potential applications were revealed in gas storage,[16,17] separation,[18] heterogeneous catalysis,[19,20] spin crossover,[21,22] drug delivery,[23] theranostics,[24] sensors,[25,26] optoelectronics,[27] etc.

Incorporation of hydrogen bonding functionalities (urea, amine, amide, thiourea, etc.) within the matrix of a CP is an excellent strategy to create a functional material which can be useful for various applications. In order to synthesize such CPs, two methodologies were used: (1) coordination-driven self-assembly of a metal ion with a ligand having programmed hydrogen bonding functionality;[28] (2) postsynthetic modification of the CP.[29] The resulting functional CP exhibited unprecedented applications in sensors,[30] gas storage,[31] selective CO_2 capture,[32] catalysis,[33] selective anion separation,[34] etc., and intriguing supramolecular assembled structures by noncovalent hydrogen bonding interactions.[28] Moreover, such functionalized CPs showed more competence in their structure-dependent applications (for example, size-selective hydrogen bond catalyst[35] compared to the nonfunctionalized

Received: March 29, 2021
Revised: May 1, 2021
Published: May 19, 2021

https://doi.org/10.1021/acs.cgd.1c00352
Cryst. Growth Des. 2021, 21, 3562−3581

CPs).[28,36−38] Among various organic building blocks, thiourea functionalized ligands attracted much attention, due to their versatile coordination ability toward metal ions through the sulfur or the nitrogen atoms or even through both of them.[39] The thiourea moiety exists in two mesomeric forms, namely, thione and thiolate, and in most of the reported compounds it showed the thiolate form (Scheme 1) due to its significant

Scheme 1. Mesomeric Forms (Thione and Thiolate) of the Ligands L1−L6[a]

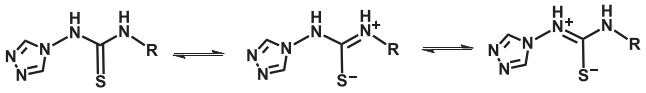

[a]R = Me, Et, prop, iso-prop, allyl, and $COOCH_2CH_3$ for **L1**, **L2**, **L3**, **L4**, **L5**, and **L6** respectively.

donor strength to the metal ion via a coordination bond.[40,41] Moreover, a Cambridge structure database (CSD)[42] search on compounds of thiourea based ligands[43,44] showed the presence of characteristic intermolecular N−H···S hydrogen bonding, with dominant N−H···O=C and N−H···S=C hydrogen bond interactions.[45,46]

Our research on the crystal engineering and functional properties of 1,2,4-triazole ligands,[47] and their CPs,[5] led us recently to investigate the structural diversities of two 1,2,4-triazole ligands, namely, 4*H*-1,2,4-triazol-4-yl-acetate and 4-(4*H*-1,2,4-triazol-4-yl)-L-propionic acid as a function of the hydrogen bonding functionality attached to the 1,2,4-triazole ligand such as the ester and carboxylic acid, respectively.[47] In these studies, the ester and carboxylic acid moiety functionalized with 1,2,4-triazole played a significant role for the self-assembly process, which led to the formation of homochiral helical chains and 2D hydrogen bonded networks, respectively. We have also recently studied the effects of conformational flexibility and hydrogen bonding of the 1,2,4-triazole ligands, on the final outcome of CPs.[6−9] In such studies, the 1,2,4-triazole ligand backbone contains hydrogen bonding carboxylic acid and ester functionalities, which help to interact with solvent molecules and counteranions, and lead to hydrogen bonding assisted self-assembled supramolecular structures. Such compounds showed unusual robustness and thermal stability, and allowed for gas adsorption[7−9] and storage of metallic mercury.[6]

Inspired by these functional CPs and their intriguing properties, we decided to functionalize the 1,2,4-triazole with a thiourea moiety (Scheme 1) and study their self-assembly properties as well as their coordination abilities toward the mercury ion due to its enormous negative impact on our environment. This study was also motivated by the following reasons: (i) thiourea molecules having nitrogen and sulfur donors atoms have shown their ability to provide variable bonding modes and structural diversity in coordination chemistry.[48,49] (ii) Thiourea is expected to participate to hydrogen bonding interactions with multiple partners (i.e., counteranions, 1,2,4-triazole groups, lattice included or metal bound solvent molecules, and even other thiourea functions). (iii) Nitrogen heteroatoms from the 1,2,4-triazole building block are suitable for coordination with metal ions and can lead to CP formation. (iv) CPs involving triazole-thiourea based ligands have not been reported, and there are no Hg(II) complexes with such ligands reported so far, thus increasing interest of the present report. (v) Metal-triazole complexes with Hg(II) ions have also been rarely reported.[50,51] (vi) Recently, we have found that for a given complex, the substituents on the ligand and complex counteranions are important components for modulating the luminescent properties of 1,2,4-triazole complexes.[51] We therefore anticipate that the current triazole-thiourea ligands are potential candidates for the detection of Hg by the formation of luminescent complexes, which is environmentally relevant as mercury and its derivatives are known to be highly toxic pollutants.[52−54]

In the present account, we introduce the crystal structures of a series of new 1,2,4-triazole ligands functionalized with thiourea **L1** to **L6** (Scheme 2) and their corresponding Hg(II)

Scheme 2. Chemical Structures of the Triazole-Thiourea Based Ligands L1−L6

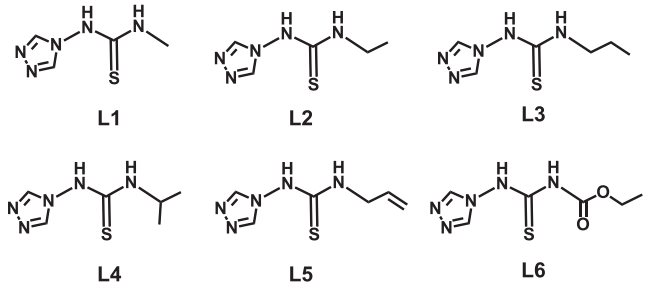

coordination compounds. We shall explore the effect of hydrogen bonding and metal coordination capability of thiourea functionality of the ligands on the supramolecular structures of the new coordination compounds. We also aim to correlate the luminescent properties of our compounds to their crystal structures. For this purpose, density function theory (DFT) calculations have been performed to assess the nature of the observed emission.

RESULTS

Synthesis and General Characterization. The ligands were prepared according to the procedure described by Bielenica et al.[55] involving the reaction of 4-amino-1,2,4-triazole and SCN-R, R being methyl (**L1**), ethyl (**L2**), propyl (**L3**), isopropyl (**L4**), allyl (**L5**), and ethyl formate (**L6**) (Scheme 3). The resulting asymmetric molecules contain a

Scheme 3. Schematic Representation of the Synthesis of the Ligands

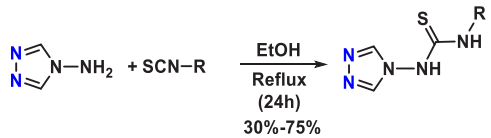

thiourea backbone with 1,2,4-triazole on the other side. This asymmetric nature allows the yield to energetically favorable conformations in their free ligand form and in their coordinated form in Hg coordination compounds.

Reaction of such ligands with mercury salts provided 10 coordination compounds which were all crystallized, using either slow evaporation or slow diffusion methods (using a branched Γ tube). The compounds were characterized by FT-IR, UV−visible, elemental analysis, and powder X-ray diffraction (PXRD). The compounds were found to be air

https://doi.org/10.1021/acs.cgd.1c00352
Cryst. Growth Des. 2021, 21, 3562−3581

and light sensitive over time, as well as hygroscopic. The crystal structures of all compounds were determined by single crystal X-ray diffraction (SXRD) providing the following formulas: {[Hg(**L1**)$_2$(**L1**$^-$)$_2$]} (**1**), {[(Hg)$_2$(**L1**)$_2$(μ_2-I)$_2$(I)$_2$]·DMSO} (**2**), {[Hg(**L2**)(μ_2-I)I]·MeOH}$_\infty$ (**3**), {[Hg$_2$(μ-**L3**$^-$)$_4$]}$_\infty$ (**4**), {[HgCl(**L4**$^-$)**L4**]·MeOH} (**5**), {[Hg$_2$(**L4**)$_2$(μ_2-I)$_2$(I)$_2$]·2MeOH} (**6**), {[Hg$_2$(μ_2-**L5**$^-$)$_4$]}$_\infty$ (**7**), {[Hg$_2$(μ_2-Cl)$_2$(**L6**$^-$)$_2$(**L6**)$_2$]} (**8**), {[Hg$_2$(μ_2-Br)$_2$(**L6**$^-$)$_2$(**L6**)$_2$]} (**9**), {[Hg$_2$(μ_2-I)$_2$(**L6**$^-$)$_2$(**L6**)$_2$]} (**10**), and {[Hg$_2$I$_3$(μ_3-**L5**′)]}$_\infty$ (**11**).

FT-IR Spectroscopy. The ligands and coordination compounds were investigated by solid-state Fourier transform infrared spectroscopy (FT-IR) over the range 4000 to 400 cm^{-1} by using KBr pellets. The comparison plots are provided in the Supporting Information (SI). The FT-IR stretching and bending frequencies of ligands and the corresponding coordination compounds showed similarity in the corresponding characteristic peaks. In the FT-IR spectra of **1** and **2**, the band at 3170 and 3134 cm^{-1}, respectively, was found to shift (3109 cm^{-1}) from the corresponding ligand **L1**. This band is attributed to the characteristic thiourea N−H stretching.[56] The characteristic IR absorption peaks belonging to the 1,2,4-triazole ring such as C−H aromatic vibrations (3088 and 2936 cm^{-1} for **L1**, 3089 and 2970 cm^{-1} for **1**, 3109 and 2938 cm^{-1} for **2**), C═C stretching (1520 and 1440 cm^{-1} for **L1**, 1512 and 1498 cm^{-1} for **1**, 1520 and 1444 cm^{-1} for **2**), and N═N stretching (1572, 1576, and 1572 cm^{-1} for **L1**, **1** and **2**, respectively) were also observed in the FT-IR spectrum of the free ligand **L1** and the corresponding complexes **1** and **2**. In addition, the band appearing at 1237 cm^{-1} due to thiourea C═S stretching in the free ligand **L1** was downward shifted to 1210 and 1183 cm^{-1} in the IR spectra of complexes **1** and **2**, respectively, indicating the coordination through the thiourea sulfur atom.[57] The coordination of Hg(II) with the S atom of the thiourea moiety of the ligand was confirmed by the IR band at 571 and 567 cm^{-1} for **1** and **2**, respectively, attributed to the Hg−S stretching frequency. Similarly, the FT-IR spectrum of compounds **3**, **4**, **5**, **6**, **7**, **8**, **9**, **10**, and **11**, and their corresponding ligands showed N−H stretching of thiourea, C−H, C═C, and N═N aromatic stretching vibrations (all the three belong to 1,2,4-thiourea functionality), thiourea C═S, and metal−ligand Hg−S stretching vibrations (Table S5).[58−61]

UV−Visible Spectroscopy. UV−visible absorption spectra of the molecules **L1**−**L6** and coordination compounds were recorded in the solid state over the range λ = 200−800 nm (spectra are shown in Supporting Information). The electronic spectra of ligands showed absorption bands exclusively in the UV region, corresponding to intraligand transitions such as $\pi-\pi^*$ and $n-\pi^*$. Similar bands were also observed in the spectra of the corresponding coordination compounds, although they were red-shifted.

Single Crystal X-ray Diffraction. Details of the data collection and refinement are given in Table S1. Topological analysis of the nets was performed using the TOPOS program package.[62,63]

Crystal Structures of Triazole-Thiourea Molecules. The ligands **L1**−**L6** are expected to show four possible conformations "*syn-syn*", "*anti-anti*", "*syn-anti*", and "*anti-syn*", in which the hydrogen atoms of thiourea function near the 1,2,4-triazole ring and alkyl/allyl/ethyl formate are on the same side (or face), opposite side, same and opposite side, opposite and same side, of thiourea, respectively (Scheme 4).

Scheme 4. Plausible Conformations of the Ligands L1−L6

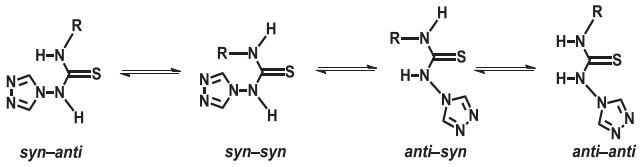

*1-Methyl-3-(4H-1,2,4-triazol-4-yl)thiourea (**L1**).* The triazole-thiourea molecule **L1** crystallizes in the centrosymmetric monoclinic $P2_1/n$ space group (Table S1). The asymmetric unit contains one molecule of **L1** and one molecule of lattice included water. From the crystal structure, it is found that the ligand is nonplanar, in which the triazole ring and the thiourea-methyl functionalities are almost perpendicular to each other [the torsion angle between the triazole and thiourea is 83.35(13)°], and shows *anti-syn* conformation (Scheme 4). The lattice water molecule stabilizes the structure by hydrogen bond interactions with three neighboring molecules of **L1**, acting as an acceptor for the N−H group of thiourea adjacent to the 1,2,4-triazole ring, while hydrogen bonding to both nitrogens of the N−N bond of **L1**, one on each side. A macrocyclic ring structure with graph set notation $R_4^4(14)$ is constructed by a N atom of the triazole, the N−H of thiourea, and the water molecule [O−H···N = 2.926(12) Å, ∠O−H−N = 148.06°; N−H···O = 2.741(14) Å, ∠N−H−O = 153.75°]. Such 0D hydrogen bonded macrocycles interact with each other through hydrogen bonding, resulting in the formation of a 2D hydrogen bonded supramolecular network structure. TOPOS analysis[62,63] suggests that it is a 2D hydrogen bonded network with Point symbol {4.8^2.10^3}{4.8^2}. The 2D hydrogen bonded network was further packed on top of each other, with the support of N−H···S hydrogen bonding involving thiourea functionalities; N−H···S is dominated by a homosynthon formation between two adjacent thiourea across an inversion center, forming a $R_2^2(8)$ ring [N−H···S = 3.3752(19) Å, ∠N−H−S = 164.46°] (Figure 1).

*1-Ethyl-3-(4H-1,2,4-triazol-4-yl)thiourea (**L2**).* The ethyl-thiourea derivative of 1,2,4-triazole **L2** also crystallizes in the centrosymmetric monoclinic space group $P2_1/n$ (Table S1), with a single molecule in the asymmetric unit. The ligand exhibits a nonplanar conformation in which the 1,2,4-triazole ring and the thiourea-ethyl functional groups were found almost orthogonal to each other (torsion angle of 84.29°). Ligand **L2** showed *syn-anti* conformation (Scheme 4), as opposed to **L1**. As a result, the observed homosynthon is formed with the NH adjacent to the triazole moiety ($R_2^2(8)$ ring), contrary to **L1** where the other NH group was acting as a donor [N−H···S = 3.248(8) Å, ∠N−H−S = 165.87°]. The other NH moiety is equally involved in a ring structure $R_2^2(14)$, linking two molecules through an interaction with a triazole nitrogen [N−H···N = 2.956(14) Å, ∠N−H−N = 152.74°]. The combination of both interactions leads to the formation of 1D *zigzag* hydrogen bonded chains (Figure 2). Interestingly, the adjacent hydrogen bonded chains are packed in a parallel fashion sustained by interactions of both triazole C−H hydrogens with a triazole N and the thiourea S atom on either side of the triazole. [C−H···N = 3.358(6) Å, ∠C−H−N = 148°; C−H···S = 3.79(10) Å, ∠C−H−S = 153°], forming a 2D layer expanding in the *ab* plane. In the *c* directions, these planes are offset in an almost orthogonal fashion, exposing the hydrophobic ethyl groups to one another.

https://doi.org/10.1021/acs.cgd.1c00352
Cryst. Growth Des. 2021, 21, 3562−3581

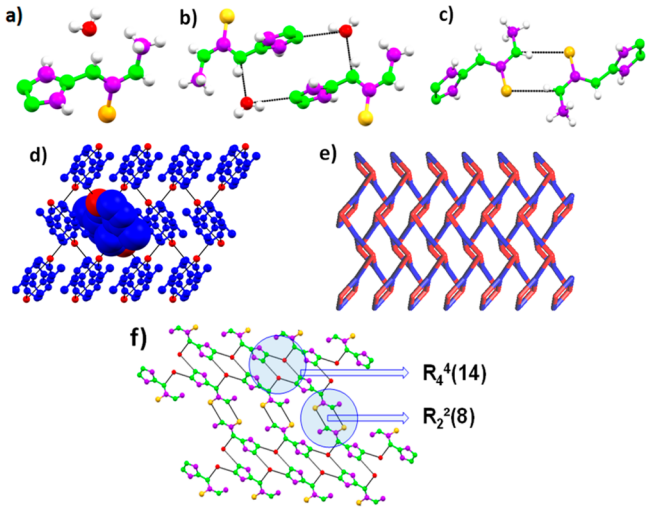

Figure 1. Crystal structure illustration of **L1**. (a) asymmetric unit of **L1**; (b) 14-membered hydrogen bonded macrocycle with graph set $R_4^4(14)$; (c) $R_2^2(8)$ ring formed by the self-complementary thiourea hydrogen bonding; (d) 2D hydrogen bonded sheet formed from the self-assembly of hydrogen bonded macrocycles (one of such macrocycles is shown in space fill model); (e) TOPOS view of 2D hydrogen bonded sheet; (f) parallel packing of 2D hydrogen bonded sheets through thiourea hydrogen bonding, displaying two distinct synthons.

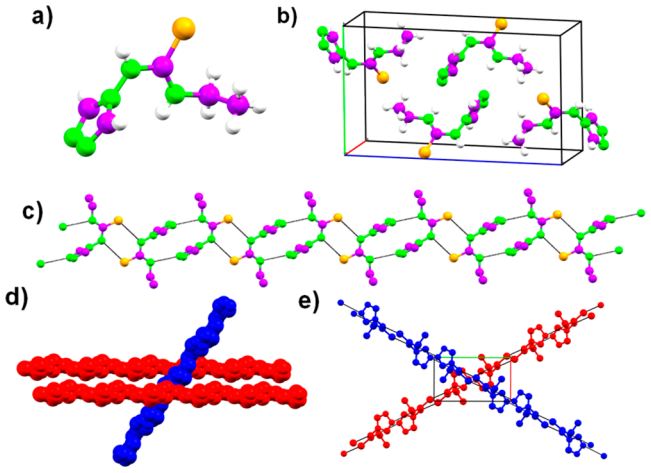

Figure 2. Crystal structure illustration of **L2**. (a) Asymmetric unit of **L2**; (b) crystal packing of **L2** molecules within the unit cell; (c) 1D *zigzag* hydrogen bonded chain, around the crystallographic axis "*a*" (hydrogen atoms were omitted for clarity); (d, e) orthogonal packing of 1D *zigzag* chains (parallel packed 1D chains are shown in red).

*1-Propyl-3-(4H-1,2,4-triazol-4-yl)thiourea (**L3**).* **L3** equally crystallizes in the centrosymmetric monoclinic space group $P2_1/n$ (Table S1). The asymmetric unit comprises one molecule of **L3**. The thiourea derivative ligand **L3** adopts a nonplanar geometry with *syn-anti* conformation (Scheme 4) as in **L2**; the triazole ring and thiourea moiety are almost orthogonal to each other with a torsion angle of 84.75°. The *syn-anti* conformation allows an identical $R_2^2(8)$ ring homosynthon as in **L2** [N−H···S = 3.256(2) Å, ∠N−H−S = 164°]. The $R_2^2(14)$ ring is also observed, similar to **L2** [N−H···N = 2.939(3) Å, ∠N−H−N = 152°]. Such hydrogen bonding leads to the formation of 1D *zigzag* hydrogen bonded chains. While **L3** exhibits similar hydrogen bonding patterns as **L2**, also forming 2D layers, consecutive 2D layers do not show an orthogonal offset but rather a parallel displacement between stacked layers in the *c* direction.

*1-Isopropyl-3-(4H-1,2,4-triazol-4-yl)thiourea (**L4**).* **L4**, isopropyl analogue and isomer to **L3**, crystallizes in the centrosymmetric triclinic $P\bar{1}$ space group (Table S1), with one molecule in the asymmetric unit. **L4** exhibits a nonplanar *syn-anti* conformation (Scheme 4) as **L2** and **L3**, in which the triazole and thiourea moiety are orthogonal to each other having a torsion angle of 86.16°. As observed in the crystal structure of **L2** and **L3**, similar hydrogen bond patterns are present: the $R_2^2(8)$ ring involving N−H···S [N−H···S = 3.225(2) Å, ∠N−H−S = 163°] as well as the $R_2^2(14)$ ring [N−H···N = 2.999(13) Å, ∠N−H−N = 155.04°]. These hydrogen bonds lead to the formation of a *zigzag* chain, and expansion of the C−H interactions of the triazole also leads to 2D layers, which in **L3** show a parallel displacement between consecutive layers (see Figure S2). A polymorph of **L4** was also obtained (**L4-poly**), also crystallizing in $P\bar{1}$, with a slightly larger unit cell volume. On the molecular level, both structures are quite similar, showing similar $R_2^2(8)$ rings between the thiourea groups. Because of subtle conformational differences, the $R_2^2(14)$ ring is however formed with the other triazole nitrogen, thus disrupting the 2D layers formed by interactions with the triazole C−H groups. In **L4-poly**, the isopropyl and the adjacent N−H are found disordered over three sites, which might indicate that the $R_2^2(14)$ ring shows less favorable hydrogen bond interactions (Figure S3).

*1-Allyl-3-(4H-1,2,4-triazol-4-yl)thiourea (**L5**).* The allyl−thiourea derivative of 1,2,4-triazole molecule **L5** crystallizes in the centrosymmetric monoclinic space group $P2_1/n$, with one molecule of **L5** in a general position (Table S1). The triazole ring and the thiourea functionalities showed nonplanar *anti-syn* (see **L1**) conformation (Scheme 4), having a torsion angle between them of around 83.89°. **L5** shows an identical $R_2^2(8)$ ring homosynthon as **L1** [N−H···S = 2.746(10) Å, ∠N−H−S = 141.73°], and the interaction with the water molecule of the NH adjacent to the triazole in **L1** is substituted by a hydrogen bond with a neighboring triazole. This interaction restricts the propagation of hydrogen bond interactions to wavy 2D layers having a hexagonal grid topology. The 2D sheets are further packed exactly on top of each other along crystallographic axis "*a*", sustained by various supramolecular interactions involving the triazole, C−H···S [C−H···S = 3.664(8) Å, ∠C−H−S = 160°] and C−H···N [C−H···N = 3.280(2) Å, ∠C−H−N = 155°] (Figure 3).

*Ethyl 2-(4H-1,2,4-Triazol-4-yl)acetate Thiourea (**L6**).* **L6** crystallizes in the orthorhombic space group *Pbca* (Table S1), with a single molecule in the asymmetric unit. **L6** exhibits nonplanar *anti-syn* conformation (see **L1** and **L5**) (Scheme 4), in which the triazole and thiourea moiety are orthogonal to each other having a torsion angle of 85.68°. In the crystal structure, **L6** molecules lack the $R_2^2(8)$ ring homosynthon involving the S atom, and **L6** is rather characterized by a bifurcated hydrogen bond engaged in an intra- and intermolecular interaction with the carbonyl oxygen of the ester group [N−H···O = 2.642(2) Å, ∠N−H−O = 133° (intra); N−H···O = 3.018(2) Å, ∠N−H−O = 132°]. **L6** undergoes further classical intermolecular hydrogen bonding through thiourea···triazole [N−H···N = 2.854 (2) Å, ∠N−H−N = 165°], and such hydrogen bonding resulted in a hexagonal-shaped macrocycle, which is the primary synthon. Extension of such hydrogen bonding resulted in a 2D

https://doi.org/10.1021/acs.cgd.1c00352
Cryst. Growth Des. 2021, 21, 3562−3581

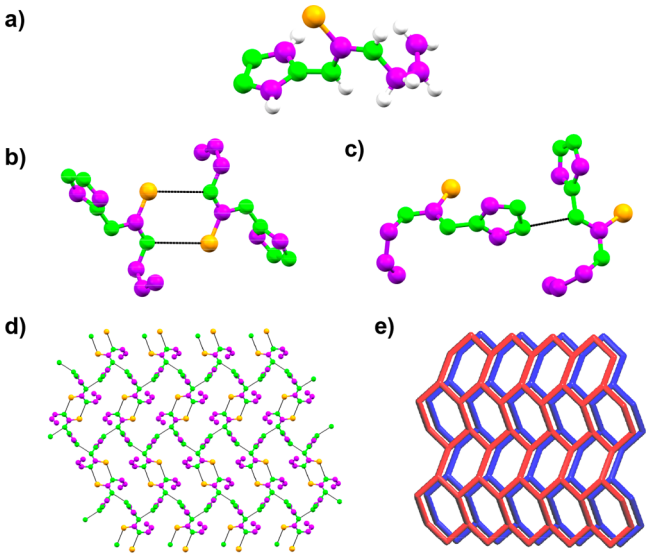

Figure 3. Crystal structure illustration of **L5**. (a) Asymmetric unit; (b) N−H···S with graph set of $R_2^2(8)$; (c) N−H···N hydrogen bonding; (d) 2D hydrogen bonded sheet formed as a result of N−H···N and N−H···S hydrogen bonding; (e) TOPOS view of overall packing of 2D hydrogen bonded networks displayed in various crystallographic axes.

hydrogen bonded hexagonal-shaped network. The 2D sheets are further packed on top of each other in an offset fashion (along crystallographic axis "*b*", sustained by C−H···N [C−H···N = 3.141(4) Å, ∠C−H−N = 121°], involving triazole (C−H)···triazole (N) (Figure 4). A solvate of **L6**, **L6_MeOH** was also found and shows the same bifurcated hydrogen. The MeOH oxygen takes the place of a triazole in the thiourea···triazole hydrogen bond found in **L6**, disrupting the 2D sheets and converting them in a zigzag layer (Figure S4).

Table S4 lists the hydrogen bond parameters for the reported ligands and complexes.

Crystal Structures of Coordination Compounds. *{[Hg(L1)$_2$(L1$^-$)$_2$]} (1).* Single crystals of complex **1** were grown from MeOH by reacting $Hg(NCS)_2$ and **L1** in a 1/3 ratio and crystallized in the tetragonal space group *I*4 (Table S1). The central Hg(II) atom is located on the crystallographic 4-fold axis, with four symmetry equivalent ligands coordinated through the S atoms, without any thiocyanato anions. Thus, the crystal structure of **1** is described as a mononuclear Hg(II) complex, tetra-coordinated by **L1**, having the formula {[Hg(**L1**)$_2$(**L1**$^-$)$_2$]}. Charge neutrality was indeed achieved by deprotonation of two ligands; as the four ligands are crystallographically identical, the charge is spread out over all four ligands, and the N−H hydrogen next to the triazole is refined as half occupied. The ligand was found to be disordered over two positions [site occupancy factor = 0.69462 and 0.30538]. The major part shows the "*syn-anti*" conformation as in the free ligand, while the minor part is found in the "*anti-anti*" conformation (Scheme 4). In the crystal structure of **1**, ligand **L1** displays an orthogonal arrangement between triazole−thiourea (dihedral angle of 89.76°) in the major part, and the minor part shows a more planar structure with a dihedral angle of 21.02°. The coordination around Hg(II) for the major and minor part is best described as a near perfect square pyramid (τ_4 = 0.95 and 1.08, respectively). We recall that τ = 0 for square pyramidal and τ = 1 for trigonal-bipyramidal arrangement, with τ is defined by the ratio $(\beta - \alpha)/60°$ where $\beta > \alpha$ are the two greatest angles of the coordination center (Figure 5).[64]

{[Hg$_2$(L1)$_2$(μ_2-I)$_2$I$_2$]·DMSO} (2). The Hg(II) binuclear complex **2**, which was prepared by reacting HgI_2 and **L1** in MeOH, crystallized in the centrosymmetric triclinic $P\bar{1}$ space group (Table S1). The unit cell contains one binuclear complex, found on an inversion center and two non-coordinated molecules of dimethyl sulfoxide (DMSO). Two iodine anions bridge the two Hg(II) centers, and the trigonal pyramidal (τ_4 = 0.78) coordination is further completed by a third iodine anion, and one molecule **L1**, coordinated through

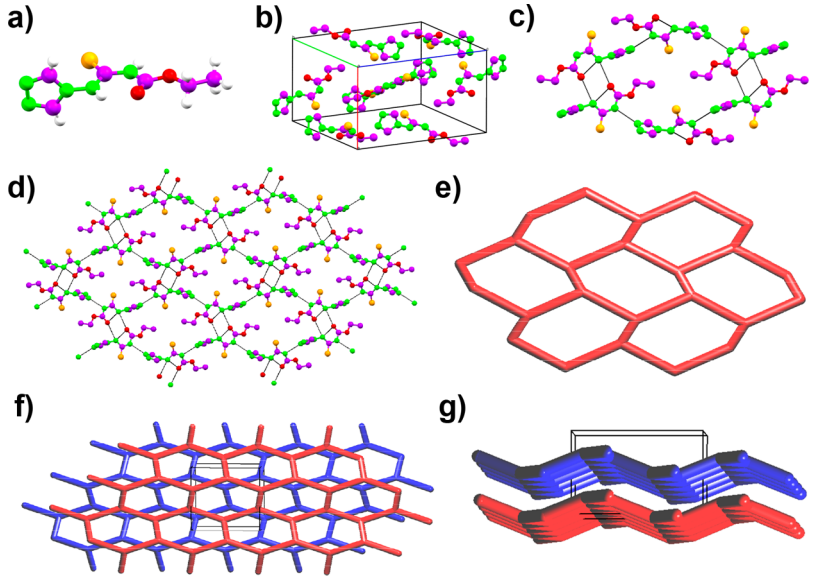

Figure 4. Crystal structure illustration of **L6**. (a) Asymmetric unit; (b) packing of **L6** molecules in unit cell; (c) hexagonal-shaped hydrogen bonded macrocycle, sustained by N−H···O and N−H···N hydrogen bonding; (d) 2D hydrogen bonded network, formed by the self-assembly of hydrogen bonded macrocycles (along crystallographic axis "*a*"); (e) TOPOS view of 2D hydrogen bonded network, displaying the hexagon-shaped topology; (f, g) offset packing of 2D sheets along various crystallographic axes.

https://doi.org/10.1021/acs.cgd.1c00352
Cryst. Growth Des. 2021, 21, 3562−3581

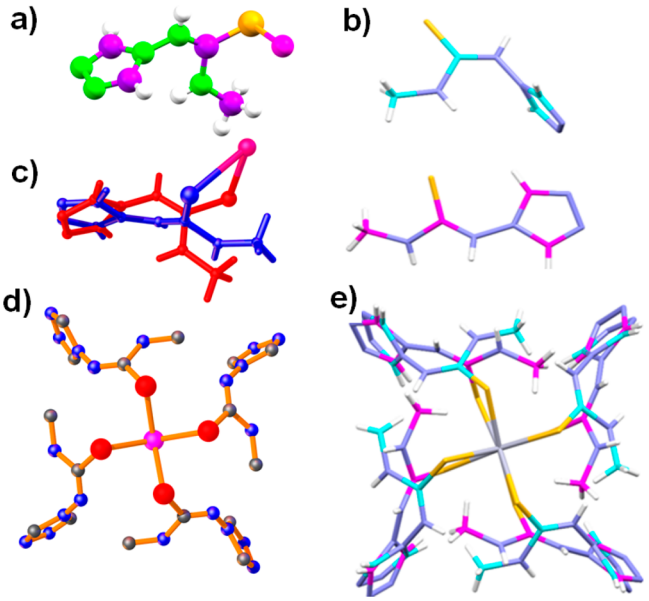

Figure 5. Crystal structure illustration of **1**. (a) Asymmetric unit; (b) stick representation of the ligand as observed in **1**; major part in cyan (top), minor part in magenta (bottom) ; (c) disorder of the ligand molecule over two positions (shown in red and blue; Hg(II) is shown in magenta); (d) mononuclear Hg(II) complex with a 1:4 metal to ligand stoichiometric ratio with coordinated sulfur atoms in red. (e) **1** showing the observed disorder.

the thiourea sulfur atom. Ligand **L1** displays a nonplanar geometry with a "*syn-anti*" conformation (Scheme 4), contrary to the *anti-syn* conformation of the free ligand and shows a dihedral angle of 88.19°, between thiourea and the triazole ring. The Hg(II) binuclear complex exhibits N−H···N hydrogen bonding [N−H···N = 2.861(2) Å, ∠N−H−N = 152.92°] between the thiourea and triazole, resulting in a 1D hydrogen bonded chain, leading to the formation of a 14-membered hydrogen bonded macrocycle of graph set $R_2^2(14)$. Additionally, $\pi\cdots\pi$ stacking interactions are present in this macrocycle between 1,2,4-triazole moieties [distance between the triazole ring centroids = 3.506 Å]. The N−H adjacent to the triazole shows a hydrogen bond to the DMSO oxygen (Figure 6).

*{[Hg(**L2**)(μ_2-I)I]·MeOH}$_\infty$ (**3**).* The coordination polymer **3**, which was prepared by reacting HgI_2 and **L2** in a 1/1 ratio in a MeOH/THF mixture, crystallized in the monoclinic space group $P2_1/c$ (Table S1). The asymmetric unit comprises one Hg(II), one molecule of **L2**, two iodide anions (both **L2** and iodide are coordinated to the metal center), and one molecule of lattice included methanol (MeOH) entrapped in the crystal lattice. The Hg(II) metal center shows a distorted trigonal pyramidal geometry [τ_4 = 0.77] in which three positions are coordinated by iodide anions, and the fourth coordination site is occupied by a S atom of the thiourea group of ligand **L2**. Two positions of the iodine atoms around every Hg(II) center are symmetry related, resulting in extended coordination polymerization, which leads to the formation of a 1D coordination polymer. This type of 1D coordination chain of {-Hg−I−Hg−I−Hg-}$_\infty$ is commonly found in Hg(II) CPs.[65,66] The ligand showed nearly identical conformation as in the free ligand **L2** (*syn-anti* conformation, RMSD 0.37 Å between the free and complexed **L2** ligand) and a similar $R_2^2(8)$ ring homosynthon as in the free **L2** ligand interactions [N−H···N = 2.977(6) Å, ∠N−H−N = 151.29°], resulting in the formation of 2D hydrogen bonded corrugated sheet-like architecture. The $\pi\cdots\pi$ stacking interactions involving the 1,2,4-triazole rings further strengthen this 2D corrugated sheet [centroid··· centroid = 3.448 Å]. In the crystal structure, the lattice included MeOH molecule is found to be hydrogen bonded with the thiourea nitrogen atom of the 2D sheet, and 1,2,4-triazole nitrogen atom of the adjacent 2D sheet [N−H···O = 2.729(12) Å, ∠N−H−O = 143.95°; O−H···N = 2.823 (8) Å, ∠N−H−O = 179.68°]; this hydrogen bonding leads to the formation of a 3D hydrogen bonded network structure (Figure 7).

*{[Hg$_2$(μ-**L3**$^-$)$_4$]}$_\infty$ (**4**).* Single crystals of the coordination polymer **4**, which was prepared by reacting $HgCl_2$ and **L3** in MeOH in a 1/1 ratio, belong to the monoclinic space group *Pn* (Table S1). The asymmetric unit contains two crystallographically independent Hg(II) ions and four crystallographically independent ligand molecules. The Hg(II) centers coordinate to four **L3** ligands through N and S atoms of 1,2,4-triazole and thiourea moieties, respectively, bridging the metal centers in all directions. The propyl group of two ligand molecules is disordered over two positions. The metal center displays a slightly distorted trigonal pyramidal geometry [τ_4 =

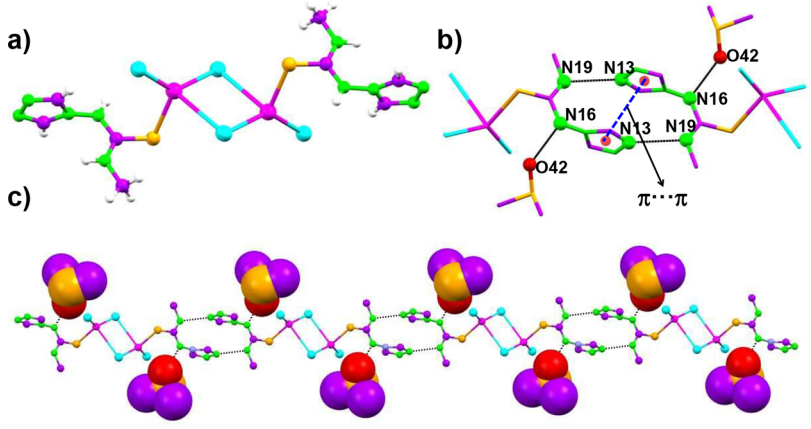

Figure 6. Crystal structure illustration of **2**. (a) Binuclear Hg(II) complex displaying the bridging of iodide anions between the Hg(II) ions; (b) hydrogen bonding and $\pi\cdots\pi$ stacking interactions in **2**; (c) 1D hydrogen bonded chain sustained by N−H···N hydrogen bonding, displaying the occlusion of DMSO (space fill model) within the interstitial space.

https://doi.org/10.1021/acs.cgd.1c00352
Cryst. Growth Des. 2021, 21, 3562−3581

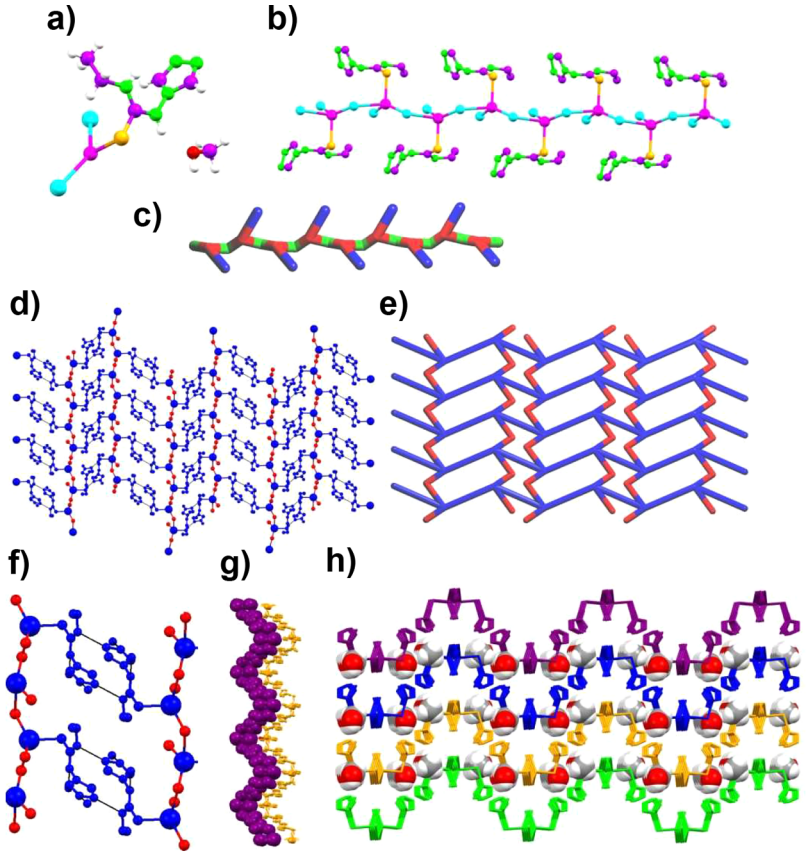

Figure 7. Crystal structure illustration of **3**. (a) Asymmetric unit containing the monomer unit of CP **3** and lattice included MeOH; (b) 1D CP displaying the {-Hg−I−Hg−I−Hg-}$_\infty$ units (Hg and I atoms are shown in magenta and cyan color, respectively), and apically coordinated ligand **L2**; (c) TOPOS view of the backbone of the CP (Hg, I, and N atom of triazole are shown in red, green, and blue); (d) extension of 1D CP to a 2D hydrogen bonded corrugated sheet structure sustained by N−H···N and $\pi\cdots\pi$ stacking interactions; (e) TOPOS view of the 2D sheet; (f) a close look of N−H···N hydrogen bonding; (g) parallel packing of 2D corrugated sheets (adjacent sheets are shown in purple and orange); (h) overall packing of 2D sheets, displaying the inclusion of MeOH (shown as a space fill model) within the interstitial space of the sheets (adjacent sheets are shown in purple, blue, orange, and green).

0.77 and 0.73]. While $HgCl_2$ was used as the starting salt, the crystal structure does not contain any chloride anions. Actually, a closer look at the crystal structure revealed that the positive charges of Hg(II) are balanced by the deprotonated form of ligand **L3** (the deprotonation takes place from the thiourea N−H, adjacent to the triazole ring). The N−N bond length involving the triazole N atom and thiourea N atom showed a slight increase from 1.386(2) Å in the free ligand to a range of 1.394(8)−1.416(11) Å in the CP, further confirming the deprotonation. The ligand **L3** exhibits *anti-syn* conformation, contrary to the free ligand that showed the *syn-anti* conformation, in which the dihedral angle between thiourea and triazole ring are in the range of 64.03−78.41°. The extended coordination of **L3** with Hg(II) resulted in the formation of a 2D square grid coordination polymer with corrugated sheet-like architecture. The thiourea N−H exhibits intramolecular hydrogen bonding with the N atom of 1,2,4-triazole (see Supporting Information), which further stabilizes the 2D corrugated sheet. Such sheets are packed on top of each other along the crystallographic axis "*a*" in a slight offset fashion, supported by various supramolecular interactions (Figure 8).

*{[HgCl(**L4**$^-$)**L4**]·MeOH}* (***5***). Single crystals of complex **5** formed by the reaction of $HgCl_2$ and **L4** in a 1/1 ratio in a MeOH/THF mixture belong to the centrosymmetric triclinic space group $P\bar{1}$ (Table S1). The asymmetric unit contains two crystallographically independent Hg atoms, each of which is coordinated to two molecules of **L4** (through the S atom of the thiourea) and to one chloride anion [Hg−Cl = 2.541(11)−2.548(8) Å; Hg−S = 2.395(5)−2.409(5)] in a distorted trigonal planar geometry, forming a mononuclear complex. For one of the discrete complexes **5**, both **L4** isopropyl groups were found disordered over two positions. The four MeOH solvent molecules found in the unit cell are also disordered over two sites. Bond valence analysis indicates that both Hg centers are in the +2 state, for which the charges are counter balanced by one Cl^- anion and a deprotonated **L4**$^-$ ligand. In all **L4** ligands, the N atom adjacent to the triazole is deprotonated, and all show the *anti-syn* conformation, contrary to the free ligand that was found in the *syn-anti* conformation, but in one of the two **L4** ligands on every Hg center the 1,2,4-triazole is protonated, forming a hydrogen bond with the deprotonated triazole of a symmetry related complex, in a $R_2^2(28)$ ring [N−H···N = 2.71(3) Å, ∠N−H−N = 161° or N−H···N = 2.70(3) Å, ∠N−H−N = 157°]. The complexes are further stabilized by intramolecular hydrogen bonds between the thiourea N−H and the Cl atom. The formation of the hydrogen bonded macrocycles results in two solvent channels running along the *a*-axis. In both channels, disordered MeOH molecules are located. The disordered nature of the MeOH

https://doi.org/10.1021/acs.cgd.1c00352
Cryst. Growth Des. 2021, 21, 3562−3581

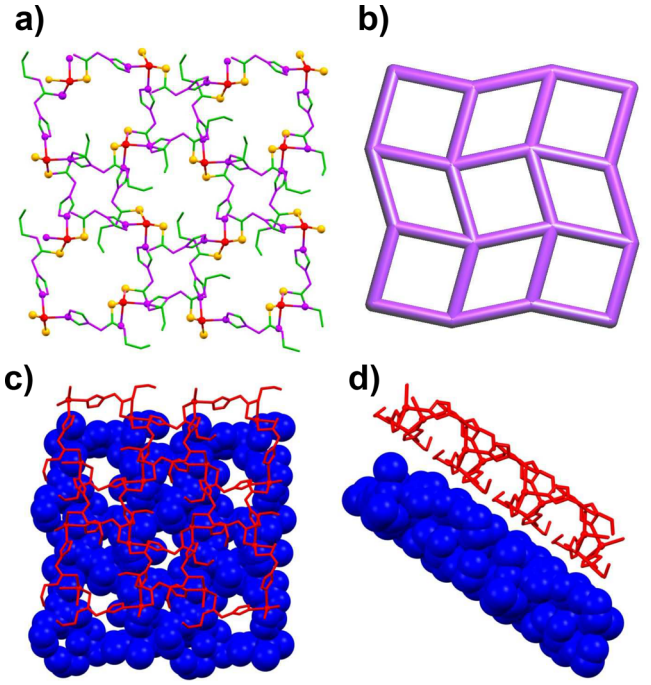

Figure 8. Crystal structure illustration of **4**. (a) 2D corrugated square grid CP, displaying the distorted trigonal pyramidal geometry of Hg(II) and the coordination modes of ligand **L3**; (b) TOPOS view of 2D corrugated square grid CP; offset packing of the square grid CPs along crystallographic axis "*a*" (c) and "*b*" (d) (adjacent CPs are shown in blue and red).

molecules and the absence of any interactions with the complexes suggest that the MeOH molecules might migrate through the channels (Figure 9).

*{[Hg_2(**L4**)$_2$(μ_2-I)$_2$$I_2$]·2MeOH} (**6**).* **6**, which was prepared by reacting HgI_2 and **L4** in a 1/1 ratio in a MeOH/THF mixture, crystallizes in a centrosymmetric triclinic space group $P\bar{1}$ (Table S1), revealing a binuclear complex formed by the self-assembly of Hg(II) salt of iodide and **L4**. The unit cell comprises a single complex **6**, with two μ_2 bridging iodine atoms and two lattice MeOH molecules. The Hg(II) metal center showed distorted tetrahedral geometry [τ_4 = 0.79], in which three coordination sites are occupied by iodide anions, and the remaining fourth was coordinated with S atom of the ligand **L4**. The ligand **L4** showed *syn-anti* conformation as in the free ligand **L4**, the dihedral angles involving the thiourea and triazole ring being 78.73°. As in the free ligand **L4**, the N atoms of the 1,2,4-triazole group of **L4** form a homodimer synthon (R_2^2(14) ring) (Figure 10) [N−H···N = 3.057(6) Å, ∠N−H−N = 144.39°], expanding into a 1D chain, which are held together by the lattice MeOH solvent molecules.

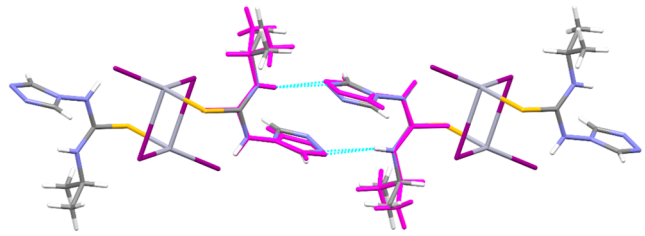

Figure 10. Stick representation of **6** showing identical hydrogen patterns as in the free ligand **L4** (superposed in magenta).

*{[Hg_2(μ_2-**L5**$^-$)$_4$]}$_\infty$ (**7**).* Single crystals of the coordination polymer **7**, which were prepared by reacting $HgCl_2$ and **L5** in a 1/1 ratio in a mixture of MeOH/THF, crystallized in the monoclinic space group *Pn* and displayed similar cell dimensions and packing as observed in **4** (Table S1). Ligands **L5** and **L3** show the same conformation in **7** and **4**, respectively, and the small conformational differences between the isostructural complexes are located between the allyl or propyl moieties. Figure 11 shows the superposition of **7** and **4**, with near perfect overlap.

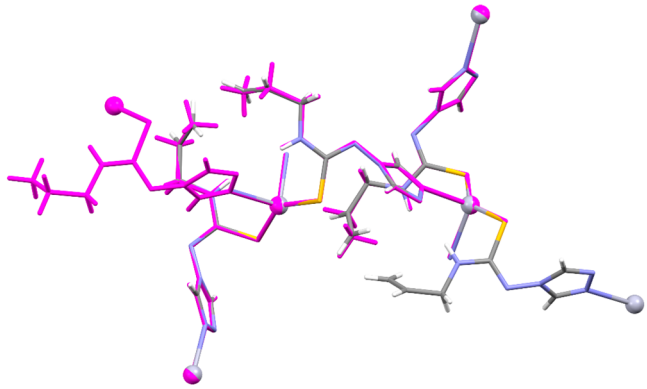

Figure 11. Superposition of **7** onto **4** (magenta), showing near perfect overlap, also between the ligands **L5** (allyl) and **L3** (propyl).

*[Hg_2(μ_2-Cl)$_2$(**L6**$^-$)$_2$(**L6**)$_2$]] (**8**), {[Hg_2(μ_2-Br)$_2$(**L6**$^-$)$_2$(**L6**)$_2$]} (**9**), and {[Hg_2(μ_2-I)$_2$(**L6**$^-$)$_2$(**L6**)$_2$]} (**10**).* The single crystals of **8**, **9**, and **10** were obtained by the reaction of **L6** with $HgCl_2$, $HgBr_2$, and HgI_2, respectively, in a 1:1 metal−ligand stoichiometric ratio. Structure determination revealed that the structures of **8**, **9**, and **10** are isomorphous and crystallized

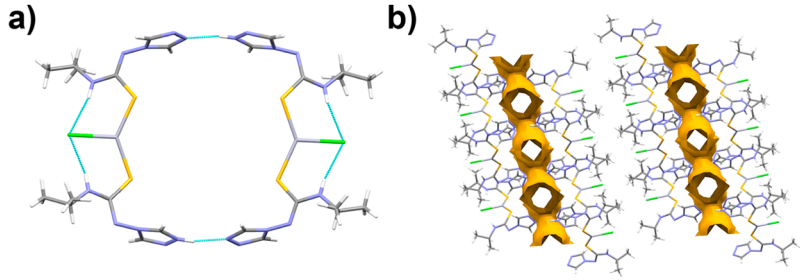

Figure 9. (a) R_2^2(28) ring macrocycle formed by hydrogen bond interactions, showing intramolecular hydrogen bonds with the chlorine atom (green) in **5**. (b) Solvent channels shown where the disordered MeOH molecules are located.

https://doi.org/10.1021/acs.cgd.1c00352
Cryst. Growth Des. 2021, 21, 3562−3581

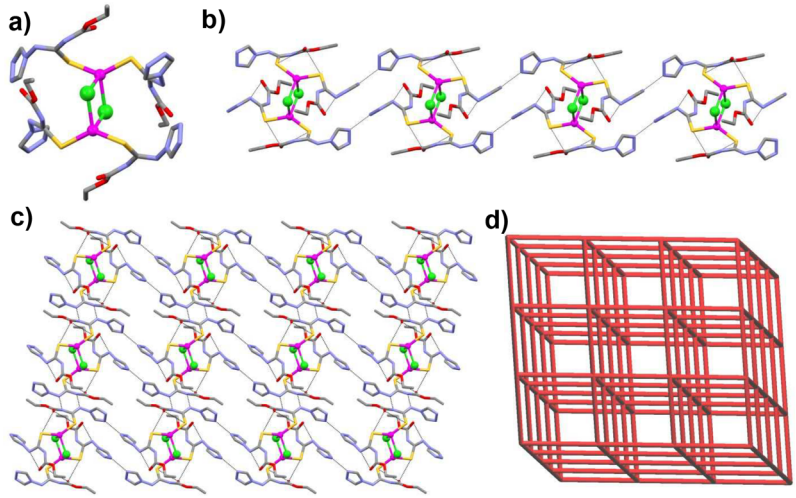

Figure 12. Crystal structure illustration of **8**. (a) Hg(II) binuclear complex **8**; (b) 1D hydrogen bonded chain; (c) 2D hydrogen bonded sheet; (d) TOPOS view of 3D hydrogen bonded network structure. Disorder on the alkyl chain was omitted for clarity.

in centrosymmetric triclinic space group $P\bar{1}$ (Table S1). The unit cell contains a single binuclear complex with two (μ_2) bridging halide anions and two S-coordinated **L6** ligands on either Hg atom (Figure 12). One of the **L6** ligands is in the *anti-anti*, the other in the *anti-syn* conformation, in which the triazole ring and thiourea moieties are almost perpendicular with dihedral angles of 78.57° & 88.20°, 80.63° & 86.21°, and 82.42° & 87.50°, for **8**, **9**, and **10** respectively. The ligand in the *anti-anti* conformation is deprotonated as $\mathbf{L6}^-$ to maintain the charge balance of the Hg(II) metal center. The Hg coordination is described as a distorted to near perfect trigonal pyramid [τ_4 = 0.79 (**8**), τ_4 = 0.82 (**9**), τ_4 = 0.84 (**10**)]. The binuclear complex self-assembled into a 3D hydrogen bonded network structure, and the main hydrogen bonds involve a dimeric $R_2^2(8)$ ring between the thiourea moieties of neighboring deprotonated **L6** ligands [N−H···N = 2.995(4)Å, ∠N−H−N = 150.34°]. The 3D network is further completed by 1D hydrogen bonded chains in the other directions with the support of N−H···N interactions [N−H···N = 2.669(11) Å, ∠N−H−N = 171.4°] between triazole groups and between the thiourea NH of a protonated and a triazole N of a neutral **L6** [N−H···N = 2.970(7)Å, ∠N−H−N = 166.84°]. Hydrogen bonds for **9** and **10** are reported in the Supporting Information.

*{[$Hg_2(\mu_3$-**L5′**)I_3]}$_\infty$ (**11**).* The reaction of the allyl-substituted thiourea−triazole ligand **L5** with HgI_2 resulted in block-shaped colorless single crystals of **11**. SC-XRD analysis revealed that crystals of **11** belong to the centrosymmetric monoclinic space group $P2_1/c$ (Table S1). Surprisingly, no **L5** was detected in the asymmetric unit. Instead, a five-membered cyclic derivative of the 1,2,4-triazole ligand (5-ethyl-1-(4*H*-1,2,4-triazol-4-yl)-imidazolidine-2-thione, **L5′**) coordinated to two Hg metal centers, was present, forming a 1D coordination polymer. Three coordinated iodide anions complete the asymmetric unit. The formation of **L5′** is presumably due to a two-step cyclization process in which **L5** reacted with HgI_2 to form a complex in the initial step, and further nucleophilic attack of $[HgI]^+$ on the allylic group (Hg−C bond) resulted in **L5′**. The proposed mechanism of the cyclization process is shown in Scheme S1. The four coordinated Hg(II) metal center shows a distorted trigonal pyramidal geometry (τ_4 = 0.78), with two iodine atoms and a thiourea S atom at the equatorial positions and the triazole N atom in the apical position; the C−Hg−I bond angle is near linear, 177.3(9)°. The Hg−I distance confirmed the oxidation states of Hg with 2.606−2.657 Å. The positive charges of the Hg are balanced by the coordinated iodide as well as the δ^+ charge on the allylic carbon atoms coordinated to Hg(II) ions. While one Hg(II) metal center shows distorted trigonal pyramidal geometry [∠N−Hg−I = 97.2(3)−101.5(3)°; ∠I−Hg−I = 143.45(6)°; ∠N−Hg−S = 89.0(3)°; ∠I−Hg−S = 105.55(10)−105.93(10)°], the Hg(II) ion coordinated to an allylic carbon atom displays a distorted linear geometry [∠C−Hg−I = 177.3(9)−177.3(9)°]. On the other hand, the trigonal pyramidal coordination geometry of Hg(II) is surrounded by a N atom of the triazole (apical position) of **L5′**, two iodide and S atoms of thiourea of ligand **L5′** (equatorial positions). The iodide anions do not participate in any bridging coordination. The extended coordination of N and S atoms of the triazole and thiourea functionalities of **L5′** with both Hg atoms leads to the formation of a 1D CP. In **L5′**, the twist angle between the five-membered rings is about 73° and the bend character leads to the formation of a 1D zigzag CP along the two-fold screw axis (Figure 13).

Photoluminescent Properties. Emission and excitation spectra of compounds **1**−**11**, as well as those of corresponding organic ligands, **L1**−**L6** were investigated in the solid state.

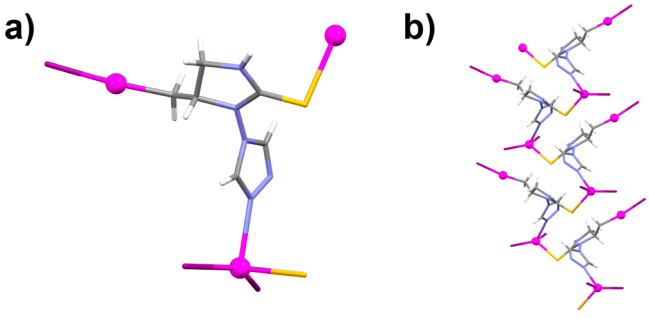

Figure 13. Crystal structure illustration of **11**. (a) Extended asymmetric unit showing the trigonal pyramidal and linear geometry around the Hg atoms, as well as coordination of **L5′**; (b) 1D zigzag CP along the 2_1-axis.

https://doi.org/10.1021/acs.cgd.1c00352
Cryst. Growth Des. 2021, 21, 3562−3581

Under UV−vis light excitation at room temperature, none of these samples exhibit a distinct photoluminescent signal. This is in contrast with the previously reported series of d^{10}-metal (Zn(II), Cd(II), Hg(II)) complexes and the related coordination polymers bearing 1,2,4-triazole-based ligands substituted at the 4-position with phenyl-containing groups.[51] In the reported case, both free organic ligands as well as the subsequent coordination compounds showed room temperature blue to blue-green photoluminescence originating from diverse emissive states, mainly related to ligand-centered electronic transitions. This can be correlated herein with the structure of **L1**−**L6** ligands which also contain 1,2,4-triazole groups, but the remaining organic parts do not contain the aromatic rings, which could result either in larger π-conjugated moieties leading to strongly emissive intraligand charge transfer (ILCT) states or in the appearance of emissive ligand-to-ligand charge transfer (LLCT) states occurring thanks to the favorable supramolecular arrangement of ligands neighboring in the crystal lattice. Despite these limitations, a distinct photoluminescence was however detected for compounds **7**, **10**, and **11** which all contain binuclear units, as well as in the corresponding free organic ligands, **L5** and **L6**, after cooling the samples to 77 K (Figures 14, 15, and 16).

Under UV light excitation, compound **7** exhibits broad emission centered at λ = 420 nm with a shoulder around λ = 520 nm (Figure 14, Table S6). This luminescence is hypsochromically shifted when compared with the free ligand **L5** showing the broad emission bands at λ = 450 nm or λ = 518 nm, depending on the excitation wavelength (Figure 14, Table S6). The ligand **L5** is built of the 1,2,4-triazole group substituted at the 4-position with the thiourea moiety finishing with the well-separated terminal allyl group (Scheme 2). Thus, the occurrence of the ILCT states can be rather excluded. Moreover, the crystal structure of **L5** (Figure 3) does not suggest the formation of supramolecular aggregates involving aromatic 1,2,4-triazole groups which could lead to the LLCT emission. Therefore, the observed photoluminescence of **L5** can be attributed to the classical ligand-centered (LC) fluorescence involving mainly the triazole π-electron system only modulated by the complex substituent. The typical UV excitation of **L5** at λ = 370 nm produces green emission related to the broadband centered at λ = 520 nm, while the deeper UV light of λ = 270 nm results in another emission band with the maximum at ca. λ = 450 nm. These emission signals can be ascribed to two different isolated LC states as clearly visible in two distinguishable bands in the excitation spectrum. A similar excitation pattern was observed for the analogous ligand of *N*-(1,2,4-triazol-4-yl)pyridine-3-carboxamide bearing aromatic triazole and pyridine moieties well separated by the carboxamide group.[51] Such a two-maxima character of the excitation spectrum remains after the coordination of **L5** by Hg(II) metal centers within the 2D coordination polymer of **7**. Therefore, the resulting emission of **7** can be assigned to the LC transitions as the formation of supramolecular aggregates of **L5** ligands, which could lead to the emissive LLCT states, is not observed in the crystal structure of this coordination network (Figure 11). Both the excitation bands as well as the resulting emission signals of **7** are significantly blue-shifted when compared with free ligand **L5** (Figure 14). It can be explained by the strong conformational modification of the ligand upon metal coordination as well as the generation of the deprotonated form of $\mathbf{L5}^-$, which balances the positive charge of Hg(II) metal centers.[67] As a result, the CIE 1931

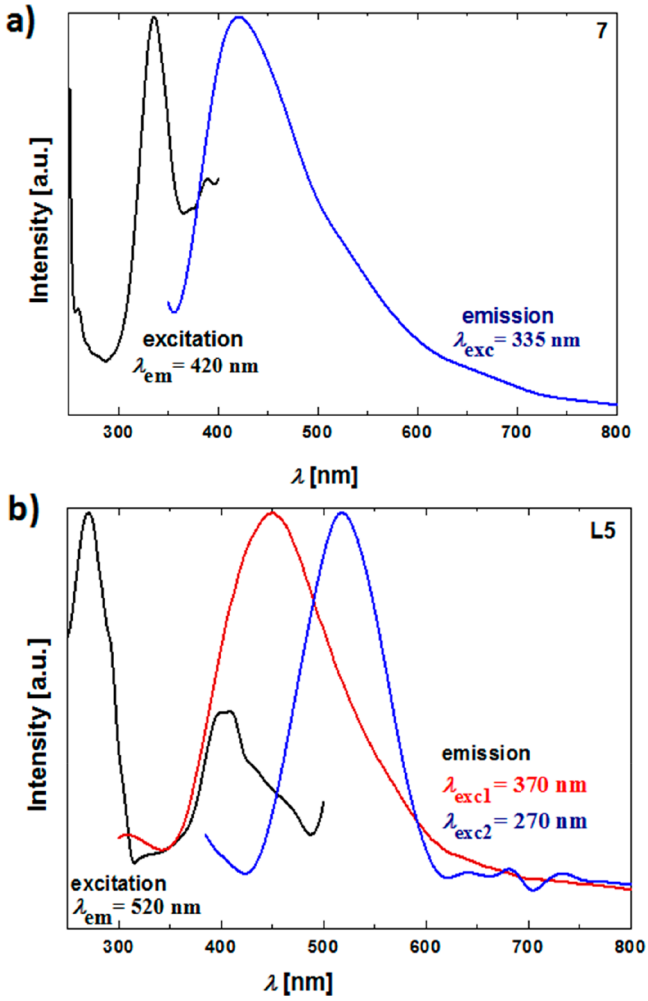

Figure 14. (a) Solid-state photoluminescence of **7** and (b) the free ligand **L5** presented through emission spectra for the indicated excitation wavelengths and excitation spectra for the indicated monitored emission wavelengths. All spectra were gathered at 77 K.

chromaticity parameters of the ligand **L5** emission of (0.228, 0.494) dramatically change to (0.215, 0.216) for the luminescent signal of **7** ,which gives the emission color shift from green to blue (Figure S1 and Table S6). Despite the strong suggestions of the LC origin of the emission in **7**, one cannot exclude the contribution of the ligand-to-metal charge transfer (LMCT) states which are accessible for Hg(II) complexes.[68,69]

The clarification of the emission mechanism in **7** is enabled by the theoretical calculations of the electronic densities of states (Figure 19b, see next section). The highest occupied states are mainly assignable to the LC electronic states. On the contrary, the lowest unoccupied states contain the main contribution from the ligand states; however, there is a non-negligible contribution from the Hg(II) electronic states. Therefore, the lowest energy optical transition, which is responsible for the observed emission pattern, can be described as a mixture of LC and LMCT (**L5** to Hg(II)) transitions. This assignment explains also the observation of a few overlapping emission components at ca. λ = 400, 450, and 540 nm, accompanied by the tail toward higher wavelengths (Figure 14).

https://doi.org/10.1021/acs.cgd.1c00352
Cryst. Growth Des. 2021, 21, 3562−3581

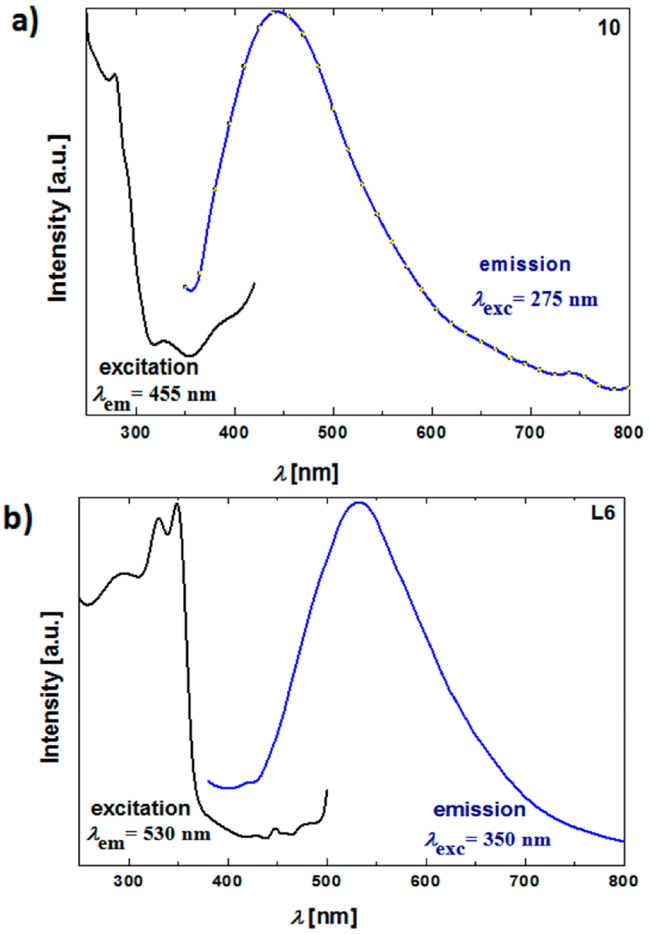

Figure 15. (a) Solid-state photoluminescence of **10** and (b) the free ligand **L6** presented through emission spectra for the indicated excitation wavelengths and excitation spectra for the indicated monitored emission wavelengths. All spectra were gathered at 77 K.

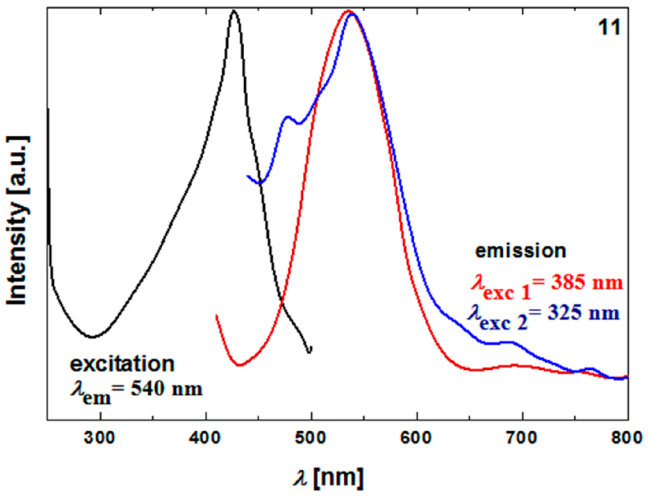

Figure 16. Solid-state photoluminescence of **11** presented through emission spectra for the indicated excitation wavelengths and excitation spectrum for the indicated monitored emission wavelength. All spectra were gathered at 77 K.

The UV-light-induced visible photoluminescence is also observed for $\{Hg(II)_2\}$ dinuclear molecules of **10** (Figure 15). The distinct emission signal was detected under the deep UV light irradiation at λ = 275 nm, which results in the broad emission band ranging from ca. λ = 350 to 600 nm, with the maximum in the blue region of the spectrum, at λ = 455 nm. Similarly to **7**, the emission of **10** is also hypsochromically shifted when compared with the free ligand **L6** exhibiting green photoluminescence with the broad emission band centered at λ = 530 nm (Table S6). The related xy CIE 1931 chromaticity parameters change from yellowish green (0.331, 0.445) for the free ligand to blue (0.219, 0.241) (Figure S1, Table S6). The ligand **L6** contains only a single aromatic group of 1,2,4-triazole substituted with long aliphatic tail involving the thiourea-ethyl(acetate) moiety (Scheme 2), and its crystal packing does not suggest the formation of any specific supramolecular aggregates (Figure 4). The ILCT or LLCT emissive states are, then, rather excluded, and the observed emission of **L6** can be assigned to LC fluorescence. Both the excitation as well as the emission patterns are shifted going from free ligand **L6** to **10**, which indicates the blue-shifted emission of a similar LC fluorescent origin. The blue-shift can be explained by the significant molecular reorientation of **L6** molecules upon metal coordination in **10** (Figure 15). There is a lack of ligand-based supramolecular stacks within the crystal structure of **10**, which could have suggested the appearance of some additional emissive LLCT states. However, the other possible sources of emission in **10**, including the charge transfer states between iodide ion and Hg(II) centers (halide-to-metal charge transfer, XMCT), between iodide and ligand **L6** (halide-to-ligand charge transfer, XLCT), or between ligand **L6** and Hg(II) centers (ligand-to-metal charge transfer, LMCT), cannot be easily excluded, as all are accessible for the family of Hg(II) halides with aromatic heterocyclic ligands.[34,46,47]

The clarification of the emission origin in **10** is also provided by the theoretical calculations of the electronic densities of states (Figure 19b, see next section). The highest occupied states are of a predominant ligand character; in particular, the S atoms of ligand **L6** contribute the most to these states. On the contrary, the lowest unoccupied states are of the mixed **L6** and Hg(II) character, indicating that the lowest energy optical transitions can be mainly described as the combination of LC and LMCT (**L6** to Hg(II)) transitions. Therefore, the emission of **10** can be assigned to the combined contributions from LC and LMCT transitions which agrees well with the observed broad emission patterns visibly consisting of a few overlapping components at ca. λ = 380, 450, and 530 nm, even with the tail toward higher wavelengths (Figure 15). One additional remark should be given to the role of iodide ions which bridge two Hg(II) centers within the dinuclear molecules of **10** (Figure 12). In the calculated DOS, there is a significant contribution from iodide ions in the energy states very near the highest occupied states, suggesting that there should be also a nonzero contribution from the halide-related XMCT/XLCT states to the overall emission. This interpretation becomes even more probable when noticing that the analogous isostructural compounds **8** and **9**, containing chloride and bromide ions, respectively, do not exhibit the emission even at 77 K. The calculated DOS of **8** (Figure S13) indicates that the characters of lowest unoccupied, as well as highest occupied states, remain similar in comparison to **10** (Figure 19b, see next section). However, the contribution of chloride-related states is positioned well below the highest occupied state, which reveals almost a purely ligand-based character. Besides, the lowest unoccupied states in **8**, which are

https://doi.org/10.1021/acs.cgd.1c00352
Cryst. Growth Des. 2021, 21, 3562−3581

still of a mixed Hg/**L6** character, are split into two distinct parts. These modifications are expected to play an important role in the observed experimental differences, the lack of detectable emission in **8** and **9** with the presence of a distinct emission signal in **10**.

Visible light emission is also observed for compound **11** (Figure 16). Under UV-to-blue light excitation, it reveals an emission band centered at ca. λ = 540 nm, which results in the green photoluminescence characterized by the (0.296, 0.550) xy CIE 1931 chromaticity parameters. This is a noticeably lower energy emission in comparison to the other investigated compounds **7** and **10** (Table S6), even though the similar structure of the organic ligand, **L5′**, which is spontaneously formed from ligand **L5**, undergoes cyclization during the crystallization process (Scheme S1). This ligand is only observed in the crystal structure of **11** and could not be isolated separately. Thus, its emission properties could not be determined. However, similar to other investigated ligands, it consists of the aromatic 1,2,4-triazole group with the 4-position substituent composed of an aliphatic ring with an additional thiocarbonyl group. Because of the lack of a large π-conjugated system, this ligand is not expected to exhibit any IL-charge-transfer transitions. In the crystal structure of **11**, there are no specific supramolecular aggregates of the ligand which could lead to the related LLCT emission. Therefore, the observed emission in **11** can be either the result of the LC fluorescence or the CT emission involving Hg(II) metal centers and organic ligand (LMCT). Alternatively, the CT emission related to the presence of iodide anions coordinated to Hg(II) centers, being also in the proximity of organic ligands (possible XMCT and XLCT states), could also be considered. The indication, on which emission pathway is realized in compound **11**, is given by the theoretical calculations of the electronic densities of states (Figure 19b, see next section). The highest occupied state was found to be mostly of a halide character, which is very different from results found for compounds **7** and **10** (see above). On the contrary, the lowest unoccupied state is strongly mixed, having both large contributions from Hg(II) metal centers (predominant one) as well as organic ligands focused mainly on the C/N-based rings rather than S atoms. As a result, the lowest energy optical transition is of XMCT and XLCT character. This indicates that the XMCT/XLCT origin of the emission property in **11** differs significantly compared to previously discussed **7** and **10** where LC and LMCT emissive transitions dominated. A similar XLCT emission was reported for the related Hg(II)-based complexes involving the simultaneous coordination of bromide anions and other triazole-containing ligands, *N*-(1,2,4-triazol-4-yl)-pyridine-3-carboxamide.[34] In that case, similarly to **11**, the resulting emission appears thanks to the appropriate supramolecular arrangement of halide ions in close vicinity of triazole-based ligands accompanying the direct coordination to Hg(II) centers. Besides, it seems that such XLCT/XMCT transitions can produce a longer wavelength emission in comparison to the LC/LMCT emissive state found in **7** and **10**.

DISCUSSION

The conformation of the ligand is, naturally, one of the important factors which affects the crystal structure of a complex, but the nature of the central metal ions, and counteranions are rather the decision making factors for the conformation of ligands in coordination compounds.[70,71] This has been shown in many cases, wherein the conformation of both the free ligand (before reacting with metal ion) and the coordination compound (of the same ligand) showed differences.[72,73] Interestingly, flexible ligands which have various plausible conformations are the key factors for successful self-assembly of important supramolecular compounds such as polycatenanes,[74] helices,[75,76] braids,[77] Borromean rings,[78] 2D square grids,[5] single-walled metal−organic nanotube,[6] and so on. However, it is a difficult task to predict the crystal structure of a coordination compound built from a flexible ligand due to (i) various possible conformations and coordination modes of these ligands; (ii) the difficulty to precisely determine their energies; and (iii) the kinetic and thermodynamic factors for the stability of the complexes and the crystal packing effect. In order to understand and precisely determine the final topological structure of the CPs, often the molecular level building block approach or a crystal engineering approach is used, in which the building blocks [supramolecular synthons[79,80]/secondary building units (SBUs)[81,82]] are capable of making predictable motifs within the resultant crystal structure.

In this work, we designed and synthesize a series of new ligands based on a thiourea backbone with 1,2,4 triazole functional groups on one side and alkyl, allyl, or ester functional groups on the other side, namely, **L1**−**L6**, as well as a polymorph of **L4** and a MeOH solvate of **L6** (Scheme 2). The ligand exhibits a degree of free rotation around the N−N bond connecting the 1,2,4-triazole and thiourea moieties ($N_{1,2,4\text{-triazole}}$−$N_{thiourea}$), and four extreme conformers can be generated by rotation around the C−N bonds within the thiourea fragment, denoted as *syn*−*anti*, *syn*−*syn*, *anti*−*syn*, and *anti*−*anti* (Scheme 3).

All ligand structures crystallize in centrosymmetric space groups forming a hydrogen bonded homosynthon over the inversion center. In **L2**, **L3**, and **L4**, this $R_2^2(8)$ ring structure is formed between the NH adjacent to the triazole moiety and the thiourea sulfur. All ligands are found in the *syn-anti* conformation (Scheme 4). **L1** and **L5** also form a similar $R_2^2(8)$ ring structure, yet involving the other thiourea NH and with the ligands in the *anti-syn* configuration. For **L1**, this situation results from the interaction with the lattice water molecule, whereas for **L5** this is the result of packing interactions. This fits very well with theoretical calculations showing that relative energies between the different conformations are quite small (see next section). In **L6**, a bifurcated hydrogen bond engaged in intra- and intermolecular interactions with the carbonyl oxygen of the ester group is observed rather than thiocarbonyl. This also imposes the *anti-syn* configuration. In all structures, the 1,2,4-triazole group is oriented almost perpendicular (83.35−86.16°) to the thiourea (Figure 17).

Although metal complexes with thiourea moieties are not uncommon (>1300 crystal structures recorded in the CSD),[42] only 64 complexes involve a mercury complex, and even fewer complexes (>50) are reported between mercury and a triazole ring. Moreover, only two ligands with the 1,2,4-triazole group directly attached to the thiourea moiety via an N−N bond are known[55] and none as a metal complex.

In all of our complexes, complexation with the Hg(II) atom occurs through the thiourea sulfur, with an offset angle Hg···S=C of 102.6° on average (range 96.6−109.9°), which is consistent with the CSD database (average 101.6° ± 5.6). The 1,2,4-triazole moiety is in general found on opposite sides of

https://doi.org/10.1021/acs.cgd.1c00352
Cryst. Growth Des. 2021, 21, 3562−3581

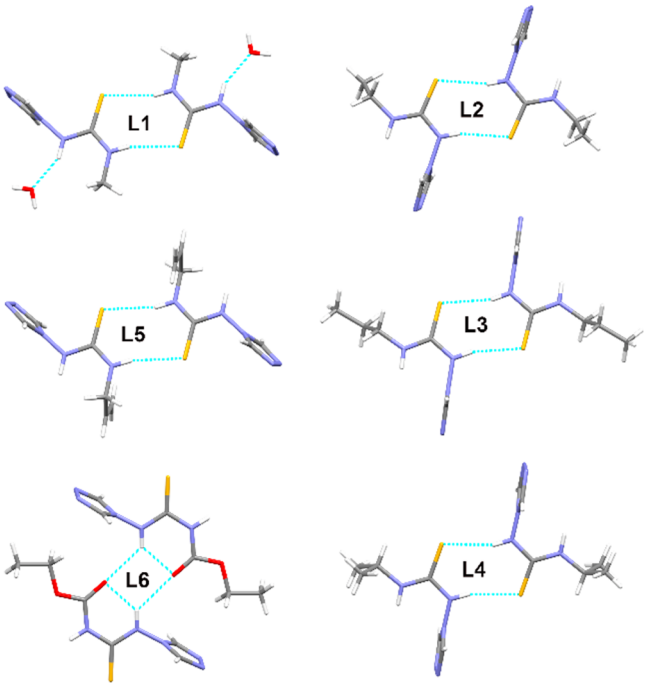

Figure 17. Stick representation of the homosynthons formed in **L1**−**L6**.

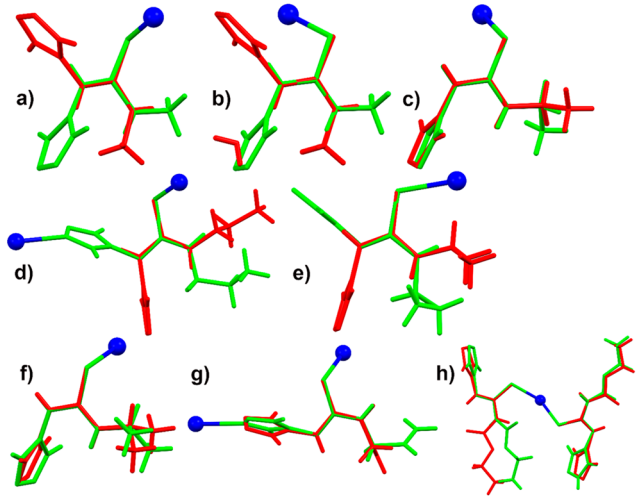

Figure 18. Overlay of ligand conformations as observed in the corresponding complexes (shown in green with the Hg atom as blue) and free ligand (shown in red color). (a) **L1** and **1**; (b) **L1** and **2** (the water molecule in the free ligand is also shown); (c) **L2** and **3**; (d) **L3** and **4**; (e) **L4** and **5**; (f) **L4** and **6**; (g) **L5** and **7**; (h) **L6** and **8** (superposition of **L6** on both the neutral and deprotonated ligand of **8** are shown).

the triazole sulfur to minimize repulsion (*syn-anti*, Scheme 2); nevertheless, the different conformations are very close in energy (see next section) and can easily convert into each other. Upon deprotonation or proton transfer from the triazole NH to the triazole ring the other configuration is observed (*anti-syn* or *anti-anti*, Scheme 2). Deprotonation allows additional coordination through the triazole moiety and the formation of coordination polymers, as observed for instance in **4** and **7**. The *syn-syn* configuration is not observed among the current series. Deprotonation or proton transfer also influences the coordination mode of the Hg center. A striking example is the difference between complexes **5** and **6**, both built from ligands **L4**. In **6**, charge neutrality is achieved by two iodine anions, forming a tetrahedrally coordinated binuclear complex, while in **5** only one chlorine anion is necessary, resulting in a trigonal complex. It is as yet unclear how the deprotonation of the ligands is achieved, as all complexes were produced in similar manner by mixing the starting salt and ligand in an equimolar ratio and crystallizing the complexes by either evaporation or convection, without any method systematically leading to deprotonation.

In Figure 18, the ligands in their free form and complexed to mercury are superposed by fitting the thiourea moieties onto each other, which also demonstrates why the *syn-syn* configuration is not observed as this would bring the triazole and alkyl ends too close to each other. More details about the coordination modes of the ligands and the corresponding bond lengths in compounds **1**−**10** are shown in Table S3. The alkyl end of the ligand has little influence on the coordination mode or type of the formed complexes, not even for ligand **L6**, where the free ligand shows inter- and intramolecular hydrogen bonding through the carbonyl oxygen.

To investigate the influence of the ligand conformation, the relative stabilities of four different conformations of **L1**, **L4**, and **L6** as depicted in Scheme 2 were calculated by DFT, with solvation effects considered from dichloromethane within the scope of a continuum solvation approximation (Figure 19a). It can be seen that, overall, all conformations of **L1** and **L4** have competitive stabilities, all lying within a 3 kcal/mol range. In the case of **L1** (*anti-syn*), the strength of, as an example, the nearest-neighbor triazole···H_2O interaction is computed to be −7.7 kcal/mol; this corroborates that the collection of intermolecular interactions in a given crystal can "override" the small stability differences between the free ligand conformers. **L6**, on the other hand, stands out because of its particularly stable *anti-syn* conformation; this preference comes from the ability to create an intramolecular hydrogen bond between the thiourea N−H and carbonyl C═O groups. In the case of **L6**, the (most stable) *anti-syn* conformation is that which appears in the **L6** crystal structure. When the thiourea N−H proton of **L6** is moved to the 1,2,4-triazole ring (labeled **L6′**), the strong conformational preference for *anti-syn* is lost because of the lack of an intramolecular hydrogen bond, and the **L6′** *anti-anti* conformation becomes competitive; the *anti-anti* and *anti-syn* conformations are the two conformers which are adopted in the structures **8**−**10**. Thus, in complexes **8**−**10**, the preferred conformers of the free ligand are also arguably preserved. As is discussed below, for every functional group (including **L6**) the scale of the intermolecular interactions is much larger than the energy differences between conformers, but the set of ligands we chose successfully maps out a rich structural space in which the conformational preferences of the ligand are sometimes preserved (in the case of **L6**, albeit with deprotonation being a decisive factor in the CP structures) and sometimes composition-dependent (in the cases of **L1** and **L4**).

One of the important factors which determines the supramolecular architectures of coordination compounds is the presence of hydrogen bonding in the ligand molecule. A design strategy based on the combination of both metal to ligand coordination bonding and hydrogen bonding in designing various metal organic supramolecular architectures is an established area of research. Interestingly, this strategy attracted many materials chemists due to the probability of

https://doi.org/10.1021/acs.cgd.1c00352
Cryst. Growth Des. 2021, 21, 3562−3581

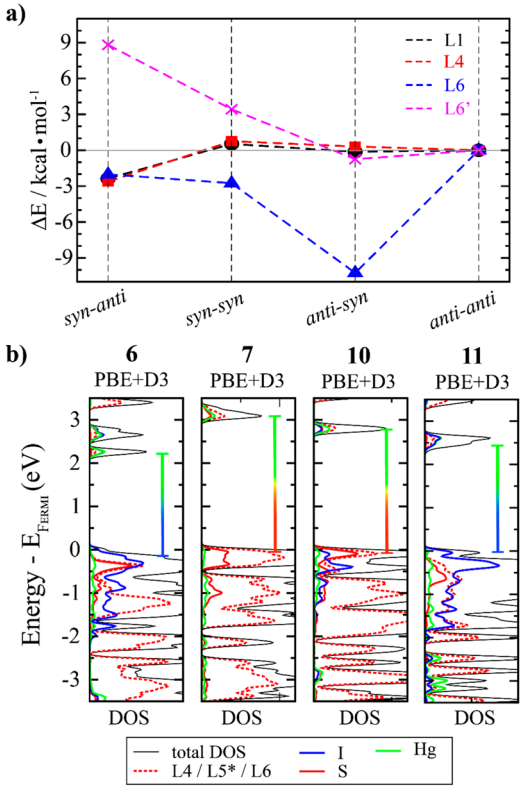

Figure 19. (a) Relative total DFT energies of the ligand conformers defined in Scheme 2; shown are **L1**, **L4**, **L6**, and **L6′**, where **L6′** was built from **L6** by moving a proton from the thiourea subunit to the triazole subunit. (b) Computed electronic densities of states (black line) for **6**, **7**, **10**, and **11** with the PBE+D3 functional; also shown, as indicated in the legend, are the atom-projected contributions to the total DOS, wherein the ligand contribution (i.e., **L4**/**L5**/**L6**) corresponds to the sum of all the atoms in the ligand. The Fermi energy is set to zero, and note that **11** does not contain **L5** (as described in the text).

structural diversities, guest entrapment supported by hydrogen bonding interactions, and functional properties having potential applications. The important benefit of using a hydrogen bonding capable ligand for the synthesis of complexes is their ability to form interchain or internetwork hydrogen bonding. The resulting materials show intriguing supramolecular structures and robustness in their framework. Thiourea is a well-known hydrogen bonding capable functional group, used in supramolecular and coordination chemistry.[83,84]

The ligands (**L1**−**L6**) contain hydrogen bonding capable groups such as thiourea, 1,2,4-triazole, and alkyl, allyl, or ester functional units. More details of hydrogen bonding of various functionalities of ligands and solvent molecules are shown in Table S2. The molecules of ligand **L1** in its free form, interact with each other through lattice included water molecules, via N−H···O, N−H···S, O−H···N, and C−H···S hydrogen bonding involving thiourea, triazole, and methyl moieties, resulting in a 2D hydrogen bonded supramolecular network. Because of the *anti-syn* conformation of ligand **L1**, thiourea··· thiourea self-complementary hydrogen bonds (N−H···S) are absent in the crystal structure. On the other hand, the N−H··· N hydrogen bonding (thiourea···triazole) in **1** resulted in a 3D network; **2** undergoes self-assembly through thiourea···triazole hydrogen bonding (N−H···N), and $\pi\cdots\pi$ stacking between the triazole rings leads to the formation of a 1D hydrogen bonded chain structure as the primary supramolecular structure, which is further extended to a 2D hydrogen bonded sheet through C−H···S and N−H···S hydrogen bonding involving thiourea and lattice included DMSO molecules. A similar kind of supramolecular structure is found in the crystal structure of **6**; the only difference is a lattice included solvent, DMSO in **2** and MeOH in **6**.

While ligand **L2** showed N−H···N and N−H···S hydrogen bonding involving the triazole and thiourea which resulted in the formation of a 1D *zigzag* chain, **3** derived from **L2** exhibited thiourea···triazole hydrogen bonding (N−H···N), and $\pi\cdots\pi$ stacking interactions (between triazole rings) resulted in 2D corrugated hydrogen bonded sheet structure, which further self-assembled to a 3D hydrogen bonded network with the support of N−H···O hydrogen bonding involving lattice included MeOH with thiourea and triazole moieties of the adjacent sheets. The ligands **L3** and **L4** also showed a similar type of hydrogen bonding and a 1D *zigzag* chain structure like **L2**. The 2D square grid **4** built from **L3**, having a corrugated sheet-like architecture, is stabilized by N−H···N intramolecular hydrogen bonding interaction, and such sheets are further self-assembled on top of each other with the support of weak van der Waals interactions. A similar type of hydrogen bonding and packing is observed in **7**. However, the ligand **L5** used for the synthesis of **7** showed thiourea ···triazole interaction through N−H···N and N−H···S hydrogen bonding and led to the formation of a 1D *zigzag* chain, which is the primary supramolecular synthon. These chains are further assembled into a 2D hydrogen bonded corrugated sheet having a hexagonal grid topology via self-complementary thiourea··· thiourea hydrogen bonding. **5** self-assembled to form a macrocycle via N···N interaction between two triazole moieties. Moreover, other supramolecular interactions such as C−H···Cl, C−H···π, and $\pi\cdots\pi$ stacking, involving isopropyl C−H with metal bound Cl, triazole C−H with a triazole ring, and thiourea C═S with a triazole ring, respectively, resulted in the formation of an oval-shaped microporous supramolecular structure. However, the inclusion of MeOH molecules blocked such pores. The self-assembly of isomorphous crystals of **8**, **9**, and **10** through N−H···N hydrogen bonding involving the protonated form of triazole, thiourea, and neutral triazole functionalities, resulted in the formation of a 3D hydrogen bonded network structure.

In order to provide physical insight into factors contributing to the stability of the reported species, extensive bonding analyses based on both cluster and periodic calculations were performed (Figures S5−S13). We shall not discuss these data in detail but provide herein only the most relevant findings. A more detailed discussion is provided in Supporting Information. First of all, ETS-NOCV data have revealed that London dispersion forces are indispensable for the overall ligand stability − ΔE_{disp} covers ∼80% of the overall stabilization in **L4**, 68% in **L3** (CH···S, CH···π, CH···HC), 51% in **L1** (CH··· S, $\pi\cdots\pi$), 48% in **L6** (σ-hole···π, NH···N), 42% in **L5** (CH···N, CH···π), and 38% in **L2** (CH···π), Figures S5−S10. As far as the corresponding metal polymers are concerned, one shall state that although dative-covalent [due to two-way electrons transfer: Lp(6s/5p, Hg) → σ*(S═C) and Lp(S) → σ*(Hg−I/S)] and electrostatically dominated Hg−S bonds are quantitatively of prime importance, they are supported by a bunch of unclassical mostly London dispersion driven noncovalent interactions, including for example: CH···π, $\pi\cdots\pi$, CH···I, and CH···HC (Figure S13); particularly, the

https://doi.org/10.1021/acs.cgd.1c00352
Cryst. Growth Des. 2021, 21, 3562−3581

latter ones are intriguing and recently under extensive debate due to a real understanding of steric-crowding in small and sizable species[85−88] (Figures S12−S13). The varying motifs that are observed as a result of the self-assemblies in **1**−**11** also result, as could be expected, in distinct valence and conduction band electronic structures, as demonstrated in Figure 19b with **6**, **7**, **10**, and **11**. The colored bars indicate the atoms in the coordination sphere of Hg which dominantly contribute to valence and conduction band energy levels, and they can be seen to change in both atom-type and length. Also, the makeup of the highest occupied energy levels varies considerably, progressing from halide-based in **6** to thiolate-character in **10** and significant triazole-character in **7**. It should be noted that the particulars of the electronic structure are sensitive the level of theory that is used (for example, the use of hybrid DFT functionals or the inclusion of spin−orbit relativistic effects), but the results clearly show that a broad distribution of self-assembled building blocks and of electronic structures is successfully realized.

CONCLUSIONS

In this work, we have explored a series of novel triazole-thiourea based ligands **L1**−**L6** and their coordination and hydrogen bonded self-assembly with Hg(II), which resulted in two mononuclear complexes **1** and **5**, five binuclear complexes **2**, **6**, **8**, **9**, and **10**, and four coordination polymers **3**, **4**, **7**, and **11**. The SC-XRD analysis of these complexes revealed that their coordination or hydrogen bonding dimensionality, topology, and supramolecular structure depend on various parameters such as conformation of ligands, counteranions, hydrogen bonding present in the ligand, and supramolecular interactions. While the self-assembly of triazole-thiourea ligands having the substituents methyl, allyl, and ethyl ester such as **L1**, **L5**, and **L6**, respectively showed a 2D hydrogen bonded corrugated sheet structure, the triazole-thiourea ligands with ethyl, propyl, and isopropyl moieties such as **L2**, **L3**, and **L4** resulted in 1D *zigzag* hydrogen bonded chains. All of these ligands showed thiourea···thiourea ($N-H_{(TU)}\cdots S_{(TU)}$) hydrogen bonding, and also other supramolecular interactions involving thiourea, triazole, and other functional groups. The ligands showed *anti-syn* and *syn-anti* conformations, when they packed into a 2D hydrogen bonded sheet and 1D chains, respectively.

The supramolecular assembly of **1** with the support of thiourea···triazole ($N-H_{(TU)}\cdots N_{(TZ)}$) interaction leads to the formation of a 3D hydrogen bonded network structure. The supramolecular structure of **2** is a 2D hydrogen bonded sheet supported with thiourea···triazole, and thiourea···DMSO. Binuclear complex **6** also has the same supramolecular structure as **2**, the only difference being the solvent of crystallization. The self-assembly of mononuclear complex **5**, initially resulted in a macrocycle, which further interacts with each other to form a 1D hydrogen bonded chain architecture, containing "I"-shaped subunits, sustained by $N-H_{(TZ)}\cdots N_{(TZ)}$. **8**, **9**, and **10** turned out to be isomorphous crystals and self-assembled into a 3D hydrogen bonded network structure supported by thiourea···thiourea ($N-H_{(TU)}\cdots S_{(TU)}$), triazole···triazole ($N-H_{(TZ)}\cdots N_{(TZ)}$), and thiourea···triazole ($N-H_{(TU)}\cdots N_{(TZ)}$). The 2D square grid **4** and **7** undergo thiourea···triazole ($N-H_{(TU)}\cdots N_{(TZ)}$) hydrogen bonding interactions and resulted in the extension of the dimensionality from 2D CP to 3D structure. The 1D CP **3** extended its self-assembly to a 2D hydrogen bonded corrugated sheet structure, with the support of various nonbonded interactions. One-dimensional zigzag CP **11** self-assembled with the support of various supramolecular interactions and led to the formation of a 3D hydrogen bonded network structure, embedding a new ligand formed *in situ*.

Among the series, **7**, **10**, and **11** were found to exhibit UV-light-induced photoluminescence in the visible range. They show the great potential of mercury(II)-halide coordination systems bearing 1,2,4-triazole derivatives in the generation of multicolored luminescence originating from remarkably diverse emissive electronic states, ranging from ligand-centered fluorescence modified upon ligand coordination and combined with organic-ligand-to-metal charge transfer (**7** and **10**), as well as halide-to-metal-charge transfer emission related to the d^{10} electronic configuration of Hg(II), combined with halide-to-ligand charge transfer taking advantage of the appropriate arrangement of organic ligands and halide ions (**11**). The origin of the emission transitions was elucidated on the basis of experimental observations compared with the emission patterns of the respective organic ligands, with the critical support of theoretical calculations of the electronic densities of states. Interestingly, all emission effects were achieved in **7**, **10**, and **11** by using relatively small 1,2,4-triazole derivatives incorporating rather short substituents in comparison to the previously reported Hg compounds with sterically expanded derivatives bearing phenyl moieties giving large π-conjugated systems and the related intraligand or ligand-to-ligand charge transfer emissive states.[29] It indicates that the reported Hg(II) halides incorporating flexible triazole-based ligands form a promising class of luminescent molecular materials offering a remarkably rich diversity of accessible and often coexisting emissive states which could be further explored toward efficient dual emissive states for applications in luminescent sensors or ratiometric luminescent thermometers. This study is also important given that several laboratories, including our team,[89] are currently designing hybrid materials including such ligands to capture Hg from aquatic media. It will help these researchers to understand the performances of their materials and improve their materials.

EXPERIMENTAL SECTION

Materials and Characterization Methods. All solvents were obtained from commercial sources. $HgBr_2$, HgI_2, $Hg(NCS)_2$, methyl thiocyanate, and allyl isothiocyanate were provided from Acros Organics. $HgCl_2$ and ethyl thiocyanate were obtained from Sigma-Aldrich. Propyl isothiocyanate, isopropyl isothiocyanate, and ethoxy carbonyl isothiocyanate were provided from TCI Chemicals. ^1H NMR spectra were recorded at 300 MHz on a Bruker AC300 instrument by using DMSO-d_6 solvent, with tetramethylsilane (TMS) as an internal standard at ambient temperature. High resolution mass spectral data were recorded in methanol on a Thermo Finnigan LCQ ion trap spectrometer in ESI mode, detecting positive ions. FT-IR spectra were recorded on a PerkinElmer 1310 spectrometer in the range 400−4000 cm^{-1} using KBr pellets. CHN analyses were performed at MEDAC Ltd.

Diffuse reflectance spectra were obtained with a PerkinElmer Lambda 9 UV/vis/NIR spectrophotometer equipped with a 60 mm integrating sphere and converted into absorption spectra by using the Kubelka−Munk function, using $BaSO_4$ as a reference. Powder X-ray diffraction patterns were recorded on a Siemens D5000 counter diffractometer working with a Cu K_α radiation (λ = 1.5148 Å) at 293 K. Photoluminescent characteristics, including solid-state emission and excitation spectra at room temperature as well as liquid nitrogen temperature, were investigated using an FS5 spectrofluorometer (Edinburgh Instruments) equipped with a Xe (150 W) arc lamp as an excitation source and a Hamamatsu photomultiplier of the R928P

https://doi.org/10.1021/acs.cgd.1c00352
Cryst. Growth Des. 2021, 21, 3562−3581

type as a detector. During these studies, the solid samples of ligands **L1**−**L6** as well as compounds **1**−**11** were measured in the form of a well-ground powder placed at the bottom of a natural quartz tube, which was inserted in the liquid nitrogen dewar mounted in the sample chamber of the spectrofluorometer. Background corrections were performed within the Fluoracle software (Edinburgh Instruments).

Syntheses. *Synthesis of Thiourea-Triazole Ligands **L1**−**L6**.* Equimolar amounts of 4-amino-1,2,4-triazole and isothiocyanate derivatives were dissolved in ethanol (25 mL) in a 100 mL round-bottom flask. The mixture was refluxed for 24 h at 60−75 °C, resulting in a pale yellow clear solution. The solution was left to cool at room temperature, and a white precipitate was collected by filtration. This product was washed with water (30 mL) and purified by recrystallization from methanol (20 mL) to obtain white crystals. The crystals were filtered, washed with ether, dried in air, and kept in a desiccator over silica gel.

*1-Methyl-3-(4H-1,2,4-triazol-4-yl) Thiourea (**L1**).* Yield: (1.31 g) 75%. Mp: 208 °C. ^{1}H NMR (300 MHz, DMSO-d_6): δ 10.75 (br, s, 1H, NH), 8.68 (s, 2H CH of trz), 8.33 (br, s, 1H, NH), 2.82 (d, 3H of CH_3). Anal. Calc. for $C_4H_7N_5S$: C, 30.57.13; H, 4.49; N, 44.50%; Found: C, 30.27; H, 4.36; N, 44.00%. IR (cm^{-1}) 3100, 1589, 1073, 614,755. MS (ESI): m/z 158.04959 $[M + H]^+$.

*1-Ethyl-3-(4H-1,2,4-triazol-4-yl) Thiourea (**L2**).* Yield: (1.51 g) 74%. Mp.: 157 °C. ^{1}H NMR (300 MHz, DMSO-d_6): δ 10.63 (br, s, 1H, NH), 8.66 (s, 2H CH of trz), 8.45 (br, s, 1H, NH), 3.46 (m, 2H of CH_2), 1.11 (t, 3H of CH_3). IR (cm^{-1}) 3156, 2904, 1567, 1180, 1053, 743, 598. Elem. Anal. Calc. for $C_4H_7N_5S$: C, 34.90; H, 5.24; N, 41.39%; Found: C, 35.07; H, 5.03; N, 40.90%. MS (ESI): m/z 172.06514 $[M + H]^+$.

*1-Propyl-3-(4H-1,2,4-triazol-4-yl) Thiourea (**L3**).* Yield: (1.04 g) 47%. Mp: 159 °C. ^{1}H NMR (300 MHz, DMSO-d_6): δ 10.59 (br, s, 1H, NH), 8.66 (s, 2H CH of trz), 8.48(br, s, 1H, NH), 3.42 (m, 2H of CH_2), 1.56 (sxt, 2H of CH_2), 0.86(t, 3H of CH_3). IR (cm^{-1}) 3112, 1572, 1179, 736, 600. Anal. Calc. for $C_4H_7N_5S$: C, 38.90; H, 5.99; N, 17.31%. Found: C, 37.93; H, 5.97; N, 17.43%. MS (ESI): m/z 186.08079 $[M + H]^+$.

*1-Isopropyl-3-(4H-1,2,4-triazol-4-yl) Thiourea (**L4**).* Yield (1.19 g) 54%. Mp: 162 °C. ^{1}H NMR (300 MHz, DMSO-d_6): δ, 10,42 (br, s, 1H, NH), 8,63 (s, 2H CH of trz), 4.42 (br, s, 1H, NH), 4.39 (m, H, CH), 1.14 (d, 6H of 2 CH_3). IR (cm^{-1}): 3055, 1591, 1040,742, 631. Anal. Calc. for $C_4H_7N_5S$: C, 38.90; H, 5.97; N, 37.30%. Found: C, 38.61; H, 5.99; N, 36.48%. MS (ESI): m/z 186.08079 $[M + H]^+$.

*1-Allyl-3-(4H-1,2,4-triazol-4-yl) Thiourea (**L5**).* Yield: (1.42 g) 65%. Mp: 111 °C. ^{1}H NMR (300 MHz, DMSO-d_6): δ, 10.74 (s, 1H, NH), 8.68 (s, 2H CH of trz), 8.65 (br, s, 1H, NH), 5.84 (d, d, 1H of CH), 5.79 (m, 2H of CH_2), 4.10 (br, s, 2H, CH_2). FT-IR (cm^{-1}) 3230, 3083, 1350, 1540, 1230, 1080, 588. Anal. Calc. for $C_4H_7N_5S$: C, 39.33; H, 4.72; N, 38.22%. Found: C, 38.22; H, 4.72; N, 38.02%. MS (ESI): m/z 184.06514 $[M + H]^+$

*Ethyl 2-(4H-1,2,4-triazol-4-yl) Acetate Thiourea (**L6**).* Yield: (1.80 g) 70%. Mp: 169 °C. ^{1}H NMR (300 MHz, DMSO-d_6): δ, 12.22 (br, s, 1H, NH), 10.83 (br, s, 1H, NH), 8.65 (s, 2H CH of trz), 4.23 (m, 2H of CH_2), 1.29 (t, 3H of CH_3).IR (cm^{-1}) 3242, 1719, 1252, 1105. Anal. Calc. for $C_4H_7N_5S$: C, 33.48; H, 4.21; N, 32.54%. Found: C, 33.03; H, 4.05; N, 32.12%.). MS (ESI): m/z 216.05497 $[M + H]^+$.

L4-poly. A total of 0.136 mmol of $HgCl_2$ (37 mg) and 0.27 mmol of **L4** (50 mg) were dissolved in a mixture of ethanol (6 mL) and THF (3 mL). The mixture was stirred for 4 h at room temperature to yield to a turbid solution which was filtrated, yielding to a clear solution which was left for slow evaporation. Plate cubic colorless crystals were filtered off after 4 days, washed with ethanol (3 mL), dried under a vacuum, and transferred into brown bottles to prevent light exposure Yield: (42 mg) 83%. Mp.: ∼160 °C. ^{1}H NMR (300 MHz, DMSO-d_6): δ, 10.41 (br, s, 1H, NH), 8.63 (s, 2H CH of trz), 8.42 (br, s, 1H, NH), 4.39 (t, 1H, CH), 3.47 (q, 2H CH_2 of Ethanol) 1.13 (d, 6H of 2 CH_3). 1.06 (d, 3H CH_3 of ethanol). IR (cm^{-1}): 3094, 1570, 1062, 746, 616.

***L6**_MeOH-1.* A total of 0.23 mmol of 74 mg of $Hg(NCS)_2$ and 0.23 mmol of **L6** (50 mg) were dissolved in a mixture of methanol (6 mL) and THF (3 mL). The mixture was stirred for 4 h at room temperature to yield to a turbid solution which was filtrated, yielding to a clear solution which was left for slow evaporation. Plate cubic colorless crystals were filtered off after 4 days, washed with methanol (3 mL), dried under a vacuum, and transferred into brown bottles to prevent light exposure. Yield: (26 mg) 52%. Mp.: ∼170 °C. ^{1}H NMR (300 MHz, DMSO-d_6): δ, 11.81 (br, s, 1H, NH), 10.83 (br, s, 1H, NH), 8.65 (s, 2H CH of trz), 4.22 (q, 2H of CH_2), 1.27 (t, 3H of CH_3). IR (cm^{-1}) 3242, 1719, 1252, 1105.

***L6**_MeOH-2.* A total of 0.23 mmol of HgI_2 (105 mg) and 0.23 mmol of **L6** (50 mg) were placed in the main arm of a Γ glass tube (Figure S7) which was filled with methanol. While the main arm was heated in an oil bath at 60 °C, colorless, block-shaped crystals deposited on the cooler arm after 6 days. These were filtered off, washed with methanol (3 mL), and dried in air. Yield: (35 mg) 70.5%. Mp.: ∼168 °C. ^{1}H NMR (300 MHz, DMSO-d_6): δ, 11.81 (br, s, 1H, NH), 8.65 (s, 2H CH of trz), 4.26 (q, 2H of CH_2), 1.27 (t, 3H of CH_3). IR (cm^{-1}) 3242, 1719, 1252, 1105.

Single crystals of **L6** were obtained as follows: 0.51 mmol of $HgCl_2$ (140 mg) and 0.26 mmol of **L6** (50 mg) were placed in the main arm of a Γ glass tube which was filled with methanol. While the main arm was heated in an oil bath at 60 °C, colorless, block-shaped crystals deposited on the cooler arm after 3 days. These were filtered off, washed with methanol (3 mL), and dried in air. Yield: (40 mg) 71%. Mp.: ∼166 °C. 1H NMR (300 MHz, DMSO-d_6): δ, 11.82 (br, s, 1H, NH), 8.65 (s, 2H CH of trz), 4.26 (q, 2H of CH2), 1.26 (t, 3H of CH_3). IR (cm^{-1}) 3325, 1819,1650, 1436, 1205, 650.

*Synthesis of Coordination Compounds. [Hg(**L1**)$_2$(**L1**$^-$)$_2$]} (**1**).* A total of 0.32 mmol of **L1** (50 mg) and 0.1 mmol of $Hg(NCS)_2$ (34 mg) were placed in the main arm of a Γ glass tube which was filled with methanol. While the main arm was heated in an oil bath at 60 °C, colorless, block-shaped crystals deposited on the cooler arm after 12 days. These were filtered off, washed with methanol (3 mL), and dried under a vacuum. Yield: (81 mg) 32%. Crystals color changed to black when exposed to air and light after 4 days. Anal. Calc. for **1**·4MeOH·10H_2O ($HgC_{20}H_{60}N_{20}O_{14}S_4$): C, 21.19; H, 5.33; N, 24.71%; Found: C, 20.94; H, 2.66; N, 24.68%. IR (KBr, cm^{-1}): 3300, 3145, 2800, 1630, 1500, 1420, 1350, 800.

*{[(Hg)$_2$(**L1**)$_2$(μ_2-I)$_2$(I)$_2$]·DMSO} (**2**).* A total of 0.23 mmol HgI_2 (106 mg) and 0.31 mmol **L1** (50 mg) were dissolved in a mixture of methanol (6 mL) and DMSO (2 mL). The mixture was stirred for 4 h at room temperature to yield to a turbid solution which was filtrated, yielding to a clear solution which was left for slow evaporation. Colorless, block-shaped crystals which were obtained after 8 days, were filtered off, washed with methanol (3 mL), and dried in air. Yield: (133 mg) 41%. Anal. Calc. for **2** ($C_{12}H_{26}Hg_2I_4N_{10}O_2S_4$): C, 10.45; H, 1.90; N, 10.15%; Found: C, 9.93; H, 1.98; N, 10.08%. IR (KBr, cm^{-1}): 3240, 3010, 2850, 2900, 1622, 1550, 1350, 1260, 830.

*{[HgI(**L2**)(μ_2-I)]·MeOH}$_\infty$ (**3**).* A total of 0.32 mmol of HgI_2 (147.5 mg) and 0.29 mmol of **L2** (50 mg) were dissolved in a mixture of methanol (6 mL) and THF (3 mL). The mixture was stirred for 4 h at room temperature to yield to a turbid solution which was filtrated, yielding to a clear solution which was left for slow evaporation. Yellow plate crystals which were obtained after 13 days were filtered off, washed with methanol (3 mL), and dried in air. Yield: (92 mg) 48%. Anal. Calc. for **3**·MeOH ($C_7H_{17}HgI_2N_5O_2S$): C, 12.19; H, 2.48; N, 10.15%; Found: C, 11.74; H, 2.25; N, 10.12%. IR (KBr, cm^{-1}): 3200, 3000, 2820, 1630, 1550, 1470, 1360, 720.

*{[(Hg)$_2$(μ-**L3**$^-$)$_4$]}$_\infty$ (**4**).* A total of 0.27 mmol of **L3** (50 mg) and 0.32 mmol of $HgCl_2$ (73 mg) were placed in the main arm of a Γ glass tube which was filled with methanol. While the main arm was heated in an oil bath at 60 °C, colorless, block-shaped crystals deposited on the cooler arm after 2 weeks. These were filtered off, washed with methanol (3 mL), and dried in an air vacuum. Yield: (53 mg) 17%. Anal. Calc. for **4**·6H_2O ($C_{24}H_{48}Hg_2N_{20}O_6S_4$): C, 23.21; H, 3.89; N, 22.55%; Found: C, 23.78; H, 3.89; N, 21.75%. IR (KBr, cm^{-1}): 3100, 3020, 2840, 1750, 1620, 1450, 1370, 1190, 890.

*{[HgCl(**L4**$^-$)**L4**]·MeOH} (**5**).* A total of 0.27 mmol of $HgCl_2$ (74 mg) and 0.27 mmol of **L4** (50 mg) were dissolved in a mixture of methanol (6 mL) and THF (3 mL). The mixture was stirred for 4 h at

https://doi.org/10.1021/acs.cgd.1c00352
Cryst. Growth Des. 2021, 21, 3562−3581

room temperature to yield to a turbid solution which was filtrated, yielding to a clear solution which was left for slow evaporation. Plate colorless crystals were filtered off after 8 days, washed with methanol (3 mL) and dried in air. Yield: (48 mg) 30%. Anal. Calc. for **5**·H_2O ($C_{13}H_{26}ClHgN_{10}O_2S_2$): C, 23.85; H, 4.00; N, 21.40%; Found: C, 23.66; H, 3.48; N, 21.71%. IR (KBr, cm^{-1}): 3360, 3120, 2870, 1620, 1490, 1380, 1250, 870.

*{[(Hg)$_2$(**L4**)$_2$(μ_2-I)$_2$(I)$_2$]·2MeOH}* ***(6)***. A total of 0.27 mmol of HgI_2 (123 mg) and 0.27 mmol of **L4** (50 mg) were dissolved in a mixture of methanol (6 mL) and THF (3 mL). The mixture was stirred for 4 h at room temperature to yield to a turbid solution which was filtrated, yielding to a clear solution which was left for slow evaporation. Yellow, block-shaped crystals were filtered off after 4 days, washed with methanol (3 mL) and dried in air. Yield: (115 mg) 32% Anal. Calc. for **6** ($C_{14}H_{30}Hg_2I_4N_{10}O_2S_2$): C, 12.52; H, 2.25; N, 10.43%. Found: C, 12.62; H, 2.14; N, 10.41%. IR (KBr, cm^{-1}): 3350, 3060, 2750, 1670, 1580, 1430, 1340, 980.

*{[(Hg)$_2$(μ_2-**L5**$^-$)$_4$]}$_\infty$* ***(7)***. A total of 0.27 mmol of $HgCl_2$ (63 mg) and 0.27 mmol of **L5** (50 mg) were dissolved in a mixture of methanol (6 mL) and THF (3 mL). The mixture was stirred for 4 h at room temperature to yield to a turbid solution which was filtrated, yielding to a clear solution which was left for slow evaporation. Colorless, block-shaped crystals were filtered off after 12 days, washed with methanol (3 mL), dried under a vacuum, and transferred into brown bottles to prevent light exposure. Yield: (117 mg) 38%. Anal. Calc. for **7**·32H_2O ($Hg_2C_{24}H_{92}N_{20}O_{32}S_4$): C, 16.93; H, 5.45; N, 16.45%; Found: C, 16.55. H, 2.02, N 16.43%. IR (KBr, cm^{-1}): 3100, 3020, 1600, 2760, 1530, 1420, 1250, 740.

*[Hg$_2$(μ_2-Cl)$_2$(**L6**$^-$)$_2$(**L6**)$_2$]]* ***(8)***. A total of 0.39 mmol of $HgCl_2$ (106 mg) and 0.23 mmol of **L6** (50 mg) were dissolved in a mixture of methanol (6 mL) and THF (3 mL). The mixture was stirred for 4 h at room temperature to yield to a turbid solution which was filtrated, yielding to a clear solution which was left for slow evaporation. Plate colorless crystals were filtered off after 10 days, washed with methanol (3 mL), dried under a vacuum, and transferred into brown bottles to prevent light exposure. Yield: (91 mg) 36%. Anal. Calc. for **8**·MeOH ($C_{25}H_{36}Hg_2Cl_2N_{20}O_9S_4$): C, 22.06; H, 2.67; N 20.58%; Found C, 22.30; H, 2.70; N 20.88%. IR (KBr, cm^{-1}): 3220, 3040, 2560, 1500, 1480, 1345, 1280, 750.

*{[Hg$_2$(μ_2-Br)$_2$(**L6**$^-$)$_2$(**L6**)$_2$]]* ***(9)***. A total of 0.23 mmol, 84 mg of $HgBr_2$ and 0.23 mmol of **L6** (50 mg) were dissolved in a mixture of methanol (6 mL) and THF (3 mL). The mixture was stirred for 4 h at room temperature to yield to a turbid solution which was filtrated, yielding to a clear solution which was left for slow evaporation. Plate colorless crystals were filtered off after 10 days, washed with methanol (3 mL), and dried under a vacuum and transferred into brown bottles to prevent light exposure. Yield: (46 mg) 17%. Anal. Calc. for **9**·44H_2O ($Hg_2C_{22}H_{120}N_{20}O_{52}Br_2$): C, 13.04; H, 5.47; N, 12.67%; Found: C, 13.56; H 2.38; N 11.93%. IR (KBr, cm^{-1}): 3210, 3035, 2620, 1560, 1480, 1330, 1270, 730.

*{[Hg$_2$(μ_2-I)$_2$(**L6**$^-$)$_2$(**L6**)$_2$]]* ***(10)***. A total of 0.16 mmol of HgI_2 (74 mg) and 0.23 mmol of **L6** (50 mg) were placed in the main arm of a Γ glass tube which was filled with methanol. While the main arm was heated in an oil bath at 60 °C, colorless, block-shaped crystals deposited on the cooler arm after 12 days. These were filtered off, washed with methanol (3 mL), and dried in air. Yield: (165 mg) 56%. Anal. Calc. for **10**·3H_2O ($C_{24}H_{38}I_2Hg_2N_{20}O_{11}S_4$): C, 18.41; H, 2.45; N, 17.89%; Found: C, 18,00; H, 2.18; N, 17.48%. IR (KBr, cm^{-1}): 3200, 3060, 1550, 1420, 1380, 1680, 810.

*{[(Hg)$_2$(**μ3-L5′**)I$_3$]}$_\infty$* ***(11)***. A total of 0.29 mmol of HgI_2 (132 mg) and 0.27 mmol of **L5′** (50 mg) were placed in the main arm of a Γ glass tube which was filled with methanol. While the main arm was heated in an oil bath at 60 °C, colorless, block-shaped crystals deposited on the cooler arm after 13 days. These were filtered off, washed with a methanol (3 mL), and dried in air. Yield: (82 mg) 32%. Anal. Calc. for **11** $C_6H_8I_3Hg_2N_5S_4$: C, 7.34; H, 1.03; N, 7.13%; Found: C, 7.28; H, 1.18; N, 7.09%. IR (KBr, cm^{-1}): 3100, 2650, 1620, 1420, 1370, 1210, 1170, 1010, 640.

Single Crystal X-ray Diffraction. Single crystal X-ray data of all compounds were collected at room temperature with a MAR345 image plate using Mo Kα (λ = 0.71069 Å) radiation. The crystals were selected from the mother solution, mounted in inert oil, and for some transferred to the cold gas stream for flash cooling (**L1**, **L5**, **L6-MeOH-1**, **8**). The unit cell parameters were refined using all the collected spots after the integration process. The data were not corrected for absorption, but the data collection mode partially takes the absorption phenomena into account. The structures were solved by direct methods and refined by full-matrix least-squares on F^2 using SHELXL97.[90,91] All the non-hydrogen atoms were refined with anisotropic temperature factors. All the H atoms were localized by Fourier difference and included in the refinement with an isotropic temperature factor.

Computational Details. All calculations were performed using density functional theory (DFT) methods within either the Vienna Ab-Initio Simulation Package (VASP),[92] for PBE+D3[93,94] models of periodic networks, or the Amsterdam Density Functional 2016 (ADF2016)[95,96] programs, for BLYP+D3 models of molecules and molecular clusters. Further details are given in the Supporting Information about the computational parameters, results from selected periodic models with a hybrid DFT functional and with spin−orbit relativistic effects, and an in-depth discussion about the ligands' interaction energies.

■ ASSOCIATED CONTENT

Supporting Information

The Supporting Information is available free of charge at https://pubs.acs.org/doi/10.1021/acs.cgd.1c00352.

Overview of NMR, mass spectrometry, IR, UV−vis, luminescence, reaction mechanism of **11**, crystallographic and theoretical modeling data (PDF)

Accession Codes

CCDC 2069121−2069129 and 2069131−2069142 contain the supplementary crystallographic data for this paper. These data can be obtained free of charge via www.ccdc.cam.ac.uk/data_request/cif, or by emailing data_request@ccdc.cam.ac.uk, or by contacting The Cambridge Crystallographic Data Centre, 12 Union Road, Cambridge CB2 1EZ, UK; fax: +44 1223 336033.

■ AUTHOR INFORMATION

Corresponding Author

Yann Garcia − *Institute of Condensed Matter and Nanosciences, Molecular Chemistry, Materials and Catalysis (IMCN/MOST), Université Catholique de Louvain, 1348 Louvain-la-Neuve, Belgium;* orcid.org/0000-0002-3105-0735; Email: yann.garcia@uclouvain.be

Authors

Houria Benaissa − *Institute of Condensed Matter and Nanosciences, Molecular Chemistry, Materials and Catalysis (IMCN/MOST), Université Catholique de Louvain, 1348 Louvain-la-Neuve, Belgium*

Nayarassery N. Adarsh − *School of Chemical Sciences, Mahatma Gandhi University, Kottayam 686560, Kerala, India;* orcid.org/0000-0003-2262-8512

Koen Robeyns − *Institute of Condensed Matter and Nanosciences, Molecular Chemistry, Materials and Catalysis (IMCN/MOST), Université Catholique de Louvain, 1348 Louvain-la-Neuve, Belgium*

Jakub J. Zakrzewski − *Inorganic Molecular Materials Group, Faculty of Chemistry, Jagiellonian University, 30-387 Krakow, Poland*

Szymon Chorazy − *Inorganic Molecular Materials Group, Faculty of Chemistry, Jagiellonian University, 30-387 Krakow, Poland;* orcid.org/0000-0002-1669-9835
James G. M. Hooper − *Department of Theoretical Chemistry, Faculty of Chemistry, Jagiellonian University, 30-060 Krakow, Poland;* orcid.org/0000-0003-3859-6172
Filip Sagan − *Department of Theoretical Chemistry, Faculty of Chemistry, Jagiellonian University, 30-060 Krakow, Poland;* orcid.org/0000-0001-5375-8868
Mariusz P. Mitoraj − *Department of Theoretical Chemistry, Faculty of Chemistry, Jagiellonian University, 30-060 Krakow, Poland;* orcid.org/0000-0001-5359-9107
Mariusz Wolff − *Institute of Condensed Matter and Nanosciences, Molecular Chemistry, Materials and Catalysis (IMCN/MOST), Université Catholique de Louvain, 1348 Louvain-la-Neuve, Belgium; Institute of Inorganic Chemistry, Johannes Kepler University Linz, 4040 Linz, Austria;* orcid.org/0000-0002-9265-7557
Smaail Radi − *LCAE, Department of Chemistry, Faculty of Sciences, University Mohamed I, 60 000 Oujda, Morocco;* orcid.org/0000-0002-5062-6904

Complete contact information is available at: https://pubs.acs.org/10.1021/acs.cgd.1c00352

Notes

The authors declare no competing financial interest.

■ ACKNOWLEDGMENTS

We acknowledge financial support from FNRS (CDR 33694457, PDR T.0095.21), Wallonie Bruxelles International (WBI COP22 Morocco, stipendium of excellence for H.B.), CNRST (ESRFC-CNRST-P10) as well as FNRS-PAN and WBI-MNiSW.

■ REFERENCES

(1) Bladin, J. A. Ueber von Dicyanphenylhydrazin abgeleitete Verbindungen. *Ber. Dtsch. Chem. Ges.* **1885**, *18*, 1544.
(2) Zhang, H.-Z.; Damu, G. L. V.; Cai, G.-X.; Zhou, C.-H. Current Developments in the Syntheses of 1,2,4-Triazole Compounds. *Curr. Org. Chem.* **2014**, *18*, 359−406.
(3) Thakur, A.; Gupta, P. S.; Shukla, P. K.; Verma, A.; Pathak, P. 1,2,4-Triazole Scaffolds: Recent Advances and Pharmacological Applications. *Int. J. Curr. Res. Aca. Rev.* **2016**, *4*, 277−296.
(4) El Rayes, S. M. Convenient Synthesis and Antimicrobial Activity of Some Novel Amino Acid Coupled Triazoles. *Molecules* **2010**, *15*, 6759−6772.
(5) Adarsh, N. N.; Dîrtu, M. M.; Guionneau, P.; Devlin, E.; Sanakis, Y.; Howard, J. A. K.; Chattopadhyay, B.; Garcia, Y. One-Dimensional Looped Chain and Two-Dimensional Square Grid Coordination Polymers: Encapsulation of Bis (1,2,4-Triazole)-*trans*-cyclohexane into the Voids. *Eur. J. Inorg. Chem.* **2019**, *2019*, 585−591.
(6) Adarsh, N. N.; Dîrtu, M. M.; Naik, A. D.; Leonard, A. F.; Campagnol, N.; Robeyns, K.; Snauwaert, J.; Fransaer, J.; Su, B. L.; Garcia, Y. Single-walled metal-organic nanotube built from a simple synthon. *Chem. - Eur. J.* **2015**, *21*, 4300−4307.
(7) Naik, A. D.; Dîrtu, M. M.; Leonard, A.; Tinant, B.; Marchand-Brynaert, J.; Su, B. L.; Garcia, Y. Engineering Three-Dimensional Chains of Porous Nanoballs from a 1,2,4-Triazole-carboxylate Supramolecular Synthon. *Cryst. Growth Des.* **2010**, *10*, 1798−1807.
(8) Dîrtu, M. M.; Neuhausen, C.; Naik, A. D.; Leonard, A.; Robert, F.; Marchand-Brynaert, J.; Su, B. L.; Garcia, Y. Superlative scaffold of 1,2,4-Triazole derivative of glycine steering linear chain to a chiral helicate. *Cryst. Growth Des.* **2011**, *11*, 1375−1384.
(9) Naik, A. D.; Tinant, B.; Leonard, A.; Marchand-Brynaert, J.; Su, B.-L.; Garcia, Y. (Di)-aminoguanidine Functionalization through Transamination: An Avenue to an Auspicious Class of Supramolecular Synthons. *Cryst. Growth Des.* **2011**, *11*, 4034−4043.
(10) Naik, A. D.; Dîrtu, M. M.; Railliet, A. P.; Marchand-Brynaert, J.; Garcia, Y. Coordination polymers and metal organic frameworks derived from 1,2,4-triazole amino acid linkers. *Polymers* **2011**, *3*, 1750−1775.
(11) Kobalz, K.; Kobalz, M.; Möllmer, J.; Junghans, U.; Lange, M.; Bergmann, J.; Dietrich, S.; Wecks, M.; Gläser, R.; Krautscheid, H. Paddle Wheel Based Triazolyl Isophthalate MOFs: Impact of Linker Modification on Crystal Structure and Gas Sorption Properties. *Inorg. Chem.* **2016**, *55*, 6938−6948.
(12) Dong, Y.; Peng, P.; Hu, B.; Su, H.; Li, S.; Pang, S. High-Density Energetic Metal−Organic Frameworks Based on the 5,5′-Dinitro-2H,2′H-3,3′-bi-1,2,4-triazole. *Molecules* **2017**, *22*, 1068.
(13) Liu, B.; Yang, T. Y.; Feng, H. J.; Zhang, Z. H.; Xu, L. A 3D chiral metal-organic framework based on left-handed helices containing 3-amino-1 H-1,2,4-triazole ligand. *J. Solid State Chem.* **2015**, *230*, 90−94.
(14) Kitagawa, S.; Kitaura, R.; Noro, S. I. Angew. Functional Porous Coordination. *Angew. Chem., Int. Ed.* **2004**, *43*, 2334−2375.
(15) Adarsh, N. N.; Novio, F.; Ruiz-Molina, D. Coordination polymers built from 1,4-bis(imidazol-1-ylmethyl)benzene: from crystalline to amorphous. *Dalton Trans.* **2016**, *45*, 11233−11255.
(16) Li, B.; Wen, H. M.; Zhou, W.; Chen, B. Porous Metal−Organic Frameworks for Gas Storage and Separation: What, How, and Why? *J. Phys. Chem. Lett.* **2014**, *5*, 3468−3479.
(17) Li, H.; Wang, K.; Sun, Y.; Lollar, C. T.; Li, J.; Zhou, H. C. Recent advances in gas storage and separation using metal−organic frameworks. *Mater. Today* **2018**, *21*, 108−121.
(18) Li, J.-R.; Sculley, J.; Zhou, H.-C. Metal−Organic Frameworks for Separations. *Chem. Rev.* **2012**, *112*, 869−932.
(19) Yu, X.; Wang, L.; Cohen, S. M. Photocatalytic metal−organic frameworks for organic transformations. *CrystEngComm* **2017**, *19*, 4126−4136.
(20) Paul, M.; Adarsh, N. N.; Dastidar, P. Secondary Building Unit (SBU) Controlled Formation of a Catalytically Active Metal−Organic Polyhedron (MOP) Derived from a Flexible Tripodal Ligand. *Cryst. Growth Des.* **2014**, *14*, 1331−1337.
(21) Garcia, Y.; Adarsh, N. N.; Naik, A. D. Crystal engineering of Fe(II) spin crossover coordination polymers derived from triazole or tetrazole ligands. *Chimia* **2013**, *67*, 411−418.
(22) Suárez-García, S.; Adarsh, N. N.; Molnár, G.; Bousseksou, A.; Garcia, Y.; Dîrtu, M. M.; Saiz-Poseu, J.; Robles, R.; Ordejón, P.; Ruiz-Molina, D. Spin-Crossover in an Exfoliated 2D Coordination Polymer and Its Implementation in Thermochromic Films. *ACS Appl. Nano Mater.* **2018**, *1*, 2662−2668.
(23) Adarsh, N. N.; Frias, C.; Ponnoth Lohidakshan, T. M.; Lorenzo, J.; Novio, F.; Garcia-Pardo, J.; Ruiz-Molina, D. Pt(IV)-based nanoscale coordination polymers: Antitumor activity, cellular up take and interactions with nuclear. *Chem. Eng. J.* **2018**, *340*, 94−102.
(24) Lu, K.; Aung, T.; Guo, N.; Weichselbaum, R.; Lin, W. Nanoscale Metal−Organic Frameworks for Therapeutic, Imaging, and Sensing Applications. *Adv. Mater.* **2018**, *30*, 1707634.
(25) Guo, Y.; Xue, S.; Dîrtu, M. M.; Garcia, Y. A. versatile iron(II)-based colorimetric sensor for the vapor-phase detection of alcohols and toxic gases. *J. Mater. Chem. C* **2018**, *6*, 3895−3900.
(26) Naik, A. D.; Robeyns, K.; Meunier, C. F.; Léonard, A. F.; Rotaru, A.; Tinant, B.; Filinchuk, Y.; Su, B. L.; Garcia, Y. Selective and reusable iron(II)-based molecular sensor for the vapor-phase detection of alcohols. *Inorg. Chem.* **2014**, *53*, 1263−1265.
(27) Wang, W.; Li, J.− L.; Jiang, C.; Hu, P.; Li, B.; Zhang, T.; Zhou, H.− C. An efficient strategy for improving the luminescent sensing performance of a terbium(III) metal−organic framework towards multiple substances. *Chem. Commun.* **2018**, *54*, 13271−13274.
(28) Adarsh, N. N.; Dastidar, P. Coordination polymers: what has been achieved in going from *innocent* 4,4′-bipyridine to bis-pyridyl ligands having a *non-innocent* backbone? *Chem. Soc. Rev.* **2012**, *41*, 3039−3060.

(29) Wang, Z.; Cohen, S. M. Postsynthetic modification of metal−organic frameworks. *Chem. Soc. Rev.* **2009**, *38*, 1315−1329.
(30) Tehrani, A. A.; Esrafili, L.; Abedi, S.; Morsali, A.; Carlucci, L.; Proserpio, D. M.; Wang, J.; Junk, P. C.; Liu, T. Urea Metal−Organic Frameworks for Nitro-Substituted Compounds Sensing. *Inorg. Chem.* **2017**, *56*, 1446−1454.
(31) Wang, X.-J.; Li, J.; Li, Q.-Y.; Li, P.-Z.; Lu, H.; Lao, Q.; Ni, R.; Shi, Y.; Zhao, Y. A urea decorated (3,24)-connected *rht*-type metal−organic framework exhibiting high gas uptake capability and catalytic activity. *CrystEngComm* **2015**, *17*, 4632−4636.
(32) Chen, C.; Zhang, M.; Zhang, W.; Bai, J. Stable Amide-Functionalized Metal−Organic Framework with Highly Selective CO_2 Adsorption. *Inorg. Chem.* **2019**, *58*, 2729−2735.
(33) Banerjee, S.; Kumar, D. P.; Bandyopadhay, S.; Adarsh, N. N.; Dastidar, P. A New Series of Cu^{II} Coordination Polymers Derived from Bis-pyridyl-bis-urea Ligands and Various Dicarboxylates and Their Role in Methanolysis of Epoxide Ring-Opening Catalysis. *Cryst. Growth Des.* **2012**, *12*, 5546−5554.
(34) Custelcean, R.; Sellin, V.; Moyer, B. A. Sulfate separation by selective crystallization of a urea-functionalized metal−organic framework. *Chem. Commun.* **2007**, *15*, 1541−1543.
(35) Roberts, J. M.; Fini, B. M.; Sarjeant, A. A.; Farha, O. K.; Hupp, J. T.; Scheidt, K. A. Urea metal-organic frameworks as effective and size-selective hydrogen-bond catalysts. *J. Am. Chem. Soc.* **2012**, *134*, 3334−3337.
(36) Li, W.; Thirumurugan, A.; Barton, P. T.; Lin, Z.; Henke, S.; Yeung, H. H. M.; Wharmby, M. T.; Bithell, E. G.; Howard, C. J.; Cheetham, A. K. Mechanical Tunability via Hydrogen Bonding in Metal−Organic Frameworks with the Perovskite Architecture. *J. Am. Chem. Soc.* **2014**, *136*, 7801−7804.
(37) Tan, K.; Jensen, S.; Zuluaga, S.; Chapman, E. K.; Wang, H.; Rahman, R.; Cure, J.; Kim, T.-H.; Li, J.; Thonhauser, T.; Chabal, Y. J. Role of Hydrogen Bonding on Transport of Coadsorbed Gases in Metal−Organic Frameworks Materials. *J. Am. Chem. Soc.* **2018**, *140*, 856−859.
(38) Alegre-Requena, J. V.; Marqués-López, E.; Herrera, R. P.; Díaz, D. D. Metal−organic frameworks (MOFs) bring new life to hydrogen-bonding organocatalysts in confined spaces. *CrystEngComm* **2016**, *18*, 3985−3995.
(39) Taheriha, M.; Ghadermazi, M.; Amani, V. Dimeric and polymeric mercury(II) complexes containing 4-methyl-1,2,4-triazole-3-thiol ligand: X-ray studies, spectroscopic characterization, and thermal analyses. *Monatsh. Chem.* **2015**, *146*, 559−569.
(40) Hollmann, K.; Oppermann, A.; Witte, M.; Li, S.; Amen, M.; Flörke, U.; Egold, H.; Henkel, G.; Herres-Pawlis, S. Copper(I) Complexes with Thiourea Derivatives as Ligands: Revealing Secrets of Their Bonding Scheme. *Eur. J. Inorg. Chem.* **2017**, *2017*, 1266−1279.
(41) Hollmann, K.; Oppermann, A.; Amen, M.; Flörke, U.; Egold, H.; Hoffmann, A.; Herres-Pawlis, S.; Henkel, G. Addressing Hydrogen Bonding Motifs by Suited Substitution of Thioureas. *Z. Anorg. Allg. Chem.* **2016**, *642*, 660−669.
(42) CSD, version 5.41, August 2020.
(43) Babashkina, M. G.; Safin, D. A.; Robeyns, K.; Garcia, Y. Complexation properties of the crown ether-containing *N*-thiophosphorylated thiourea towards Ni^{II}. *Dalton Trans.* **2012**, *41*, 1451−1453.
(44) Safin, D. A.; Babashkina, M. G.; Robeyns, K.; Garcia, Y. Halogen anion-induced formation of $[(PdLX)_2]$ (X = Cl^-,Br^-, I^-) vs. $[PdL_2]$ (L = [6 $MeO(O)CC_6H_4NHC(S)NP(S)(OiPr)_2$]−): Reversible photoinduced cis/trans isomerization of $[PdL_2]$. *Dalton Trans.* **2012**, *41*, 4324−4327.
(45) Saeed, A.; Bolte, M.; Erben, M. F.; Pérez, H. Intermolecular interactions in crystalline 1-(adamantane-1-carbonyl)-3-substituted thioureas with Hirshfeld surface analysis. *CrystEngComm* **2015**, *17*, 7551−7563.
(46) Saeed, A.; Florke, U.; Erben, M. F. A review on the chemistry, coordination, structure and biological properties of 1-(acyl/aroyl)-3-(substituted) thioureas. *J. Sulfur Chem.* **2014**, *35*, 318−355.
(47) Dîrtu, M. M.; Adarsh, N. N.; Naik, A. D.; Robeyns, K.; Garcia, Y. Supramolecular homochiral helicity and zigzag hydrogen bonding networks in 1,2,4-triazole derived amino ester and amino acid. *New J. Chem.* **2016**, *40*, 9025−9029.
(48) Bowmaker, G. A.; Hanna, J. V.; Pakawatchai, C.; Skelton, B. W.; Thanyasirikul, Y.; White, A. H. Crystal structures and vibrational spectroscopy of copper(I) thiourea complexes. *Inorg. Chem.* **2009**, *48*, 350−368.
(49) Casas, J. S.; García-Tasende, M. S.; Sordo, J. Cu(II) Benzoylpyridine Thiosemicarbazone Complexes: Inhibition of Human Topoisomerase IIα and Activity against Breast Cancer Cells. *Coord. Chem. Rev.* **2000**, *209*, 197−261.
(50) Liu, K.; Shi, W.; Cheng, P. The coordination chemistry of Zn(II), Cd(II) and Hg(II) complexes with 1,2,4-triazole derivatives. *Dalton Trans.* **2011**, *40*, 8475.
(51) Benaissa, H.; Wolff, M.; Robeyns, K.; Knor, G.; Van Hecke, K.; Campagnol, N.; Fransaer, J.; Garcia, Y. Syntheses, crystal structures, luminescent properties, and electrochemical synthesis of group 12 element coordination polymers with 4-substituted-1,2,4-triazole ligands. *Cryst. Growth Des.* **2019**, *19*, 5292−5307.
(52) Guo, X. F.; Qian, X. H.; Jia, L. H. A Highly Selective and Sensitive Fluorescent Chemosensor for Hg^{2+} in Neutral Buffer Aqueous Solution. *J. Am. Chem. Soc.* **2004**, *126*, 2272.
(53) Yu, Y.; Lin, L.-R.; Yang, K.-B.; Zhong, X.; Huang, R.-B.; Zheng, L.-S. *p*-Dimethylaminobenzaldehyde thiosemicarbazone: A simple novel selective and sensitive fluorescent sensor for mercury(II) in aqueous solution. *Talanta* **2006**, *69*, 103.
(54) Wang, L.; Zhu, X.- J.; Wong, W.-Y.; Guo, J.- P.; Wong, W.-K.; Li, Z.-Y. J. Dipyrrolylquinoxaline-bridged Schiff bases: a new class of fluorescent sensors for mercury(ii). *Dalton Trans.* **2005**, 3235.
(55) Bielenica, A.; Kedzierska, E.; Fidecka, S.; Maluszynska, H.; Miroslaw, B.; Koziol, A. E.; Stefanska, J.; Madeddu, S.; Giliberti, G.; Sanna, G.; Struga, M. Synthesis, antimicrobial and pharmacological evaluation of thiourea derivatives of 4H-1,2,4-triazole. *Lett. Drug. Discovery* **2015**, *12*, 263.
(56) Zhang, Y.-M.; Yang, Li-Zi; Lin, Q.; Wei, T.-B. Synthesis and crystal structure of bis{(μ-chloro)-chloro-[N-benzoyl-N′-(2-hydroxyethyl)thiourea]mercury(II)}. *J. Coord. Chem.* **2005**, *58*, 1675−1679.
(57) Glaser, R. E. Organic Spectroscopy, Vibrational Spectroscopy Tutorial: Sulfur and Phosphorus, Carissa Hampton Dustin Demoin, Fall 2010.
(58) Samiei Paqhaleh, D. M.; Aminjanov, A. A.; Amani, V. Dimeric and polymeric mercury(II) complexes containing 4-methyl-1,2,4-triazole-3-thiol ligand: X-ray studies, spectroscopic characterization, and thermal analyses. *J. Inorg. Organomet. Polym. Mater.* **2015**, *146*, 559−569.
(59) Jiang, Y. L.; Wang, Y. L.; Lin, J. X.; Liu, Q. Y.; Lu, Z. H.; Zhang, N.; Wei, J. J.; Li, L. Q. Syntheses, structures and properties of coordination polymers of cadmium(ii) with 4-methyl-1,2,4-triazole-3-thiol ligand. *CrystEngComm* **2011**, *13*, 1697−1706.
(60) Jolley, J.; Cross, W. I.; Pritchard, R. G.; McAuliffe, C. A.; Nolan, K. B. Synthesis and characterisation of mercaptoimidazole, mercaptopyrimidine and mercaptopyridine complexes of platinum(II) and platinum(III). The crystal and molecular structures of tetra(2-mercaptobenzimidazole)- and tetra(2-mercaptoimidazole)platinum-(II) chloride. *Inorg. Chim. Acta* **2001**, *315*, 36−43.
(61) Bellamy, L. J. *The Infrared Spectra of Complex Molecules*, 3rd ed.; Chapman and Hall: London, 1975.
(62) Blatov, V. A.; Proserpio, D. M. *TOPOS 4.0*, A Program Package for Multipurpose Crystallochemical Analysis, http://www.topos.ssu.samara.ru/.
(63) Blatov, V. A. Multipurpose crystallochemical analysis with the program package TOPOS,. *IUCr Comp Comm Newsl.* **2006**, *4*, 38.
(64) Addison, A. W.; Rao, T. N.; Reedijk, J.; van Rijn, J.; Verschoor, G. C. Synthesis, structure, and spectroscopic properties of copper(II) compounds containing nitrogen−sulphur. *J. Chem. Soc., Dalton Trans.* **1984**, 1349−1356.
(65) Khalaji, A. D.; Bahramian, B.; Jafari, K.; Fejfarova, K.; Dusek, M. *Russ. J. Coord. Chem.* 2013, *39*, 877−884.

https://doi.org/10.1021/acs.cgd.1c00352
Cryst. Growth Des. 2021, 21, 3562−3581

(66) Morsali, A.; Masoomi, M. Y. *Coord. Chem. Rev.* **2009**, *253*, 1882−1905.
(67) Volpi, G.; Priola, E.; Garino, C.; Daolio, A.; Rabezzana, R.; Benzi, P.; Giordana, A.; Diana, E.; Gobetto, R. Blue fluorescent zinc(II) complexes based on tunable imidazo[1,5-a]pyridines. *Inorg. Chim. Acta* **2020**, *509*, 119662.
(68) Cho, M.; Shin, H. J.; Kusumahastuti, D. K. A.; Yeo, H.; Min, K. S. Monomeric and tetrameric mercury (II) complexes with iodo and N_2O_2/N_3O ligands: Structure and blue luminescence. *Inorg. Chim. Acta* **2020**, *511*, 119789.
(69) Liu, D. S.; Sui, Y.; Ye, G.-M.; Wang, H -y.; Liu, J.-Q.; Chen, W.-T. Synthesis, structures and properties of three mercury coordination polymers based on 5-methyltetrazolate ligand. *J. Solid State Chem.* **2018**, *263*, 182.
(70) Ohi, H.; Tachi, Y.; Itoh, S. Supramolecular and Coordination Polymer Complexes Supported by a Tripodal Tripyridine Ligand Containing a1,3,5-Triethylbenzene Spacer. *Inorg. Chem.* **2004**, *43*, 4561−4563.
(71) Duriska, M. B.; Neville, S. M.; Batten, S. R. Variable length ligands: a new class of bridging ligands for supramolecular chemistry and crystal engineering. *Chem. Commun.* **2009**, 5579−5581.
(72) Adarsh, N. N.; Kumar, D. K.; Dastidar, P. Zn(II) metal−organic frameworks (MOFs) derived from a bis-pyridyl-bis-urea ligand: effects of crystallization solvents on the structures and anion binding properties. *CrystEngComm* **2008**, *10*, 1565−1573.
(73) Adarsh, N. N.; Kumar, D. K.; Suresh, E.; Dastidar, P. Coordination polymers derived from a bis-pyridyl-bis-amide ligand: Supramolecular structural diversities and anion binding properties. *Inorg. Chim. Acta* **2010**, *363*, 1367−1376.
(74) Lan, Y.-Q.; Li, S -Li.; Qin, J.-S.; Du, D.-Y.; Wang, X.-L.; Su, Z.-M.; Fu, Q. Self-Assembly of 2D → 2D Interpenetrating Coordination Polymers Showing Polyrotaxane- and Polycatenane-like Motifs: Influence of Various Ligands on Topological Structural Diversity. *Inorg. Chem.* **2008**, *47*, 10600−10610.
(75) Ezuhara, T.; Endo, K.; Aoyama, Y. Helical Coordination Polymers from Achiral Components in Crystals. Homochiral Crystallization, Homochiral Helix Winding in the Solid State, and Chirality Control by Seeding. *J. Am. Chem. Soc.* **1999**, *121*, 3279−3283.
(76) Banerjee, S.; Adarsh, N. N.; Dastidar, P. An unprecedented all helical 3D network and a rarely observed non-interpenetrated octahedral network in homochiral Cu(II) MOFs: effect of steric bulk and $\pi-\pi$ stacking interactions of the ligand backbone. *CrystEngComm* **2009**, *11*, 746−749.
(77) Moon, S. Y.; Kim, E.; Noh, T. H.; Lee, Y. A.; Jung, O. S. Triple-meso helices as alcohol reservoirs and discriminators: structural properties and thermal behaviors of silver(I) coordination molecular braids containing diethylbis(4-pyridyl)silanes. *Dalton Trans.* **2013**, *42*, 13974−13980.
(78) Adarsh, N. N.; Dastidar, P. A Borromean Weave Coordination Polymer Sustained by Urea−Sulfate Hydrogen Bonding and Its Selective Anion Separation Properties. *Cryst. Growth Des.* **2010**, *10*, 483−487.
(79) Sekiya, R.; Nishikiori, S-i; Kuroda, R. Combination between metal−ligand coordination and hydrogen bond interaction: a facile route for the construction of 3D coordination networks with the ability to include relatively large aromatic molecules. *CrystEngComm* **2009**, *11*, 2251−2253.
(80) Applegarth, L.; Goeta, A. E.; Steed, J. W. Influence of hydrogen bonding on coordination polymer assembly. *Chem. Commun.* **2005**, 2405−2406.
(81) Hollmann, K.; Oppermann, A.; Witte, M.; Li, S.; Amen, M.; Flörke, U.; Egold, H.; Henkel, G.; Herres-Pawlis, S. Copper(I) Complexes with Thiourea Derivatives as Ligands: Revealing Secrets of Their Bonding Scheme. *Eur. J. Inorg. Chem.* **2017**, *2017*, 1266−1279.
(82) Lu, H.; Zhu, Y.; Chen, N.; Gao, Y.; Guo, X.; Li, G.; Tang, M. Ligand-Directed Assembly of a Series of Complexes Bearing Thiourea-Based Carboxylates. *Cryst. Growth Des.* **2011**, *11*, 5241−5252.
(83) Succaw, G. L.; Weakley, T. J. R.; Han, F.; Doxsee, K. M. Crystal Engineering with Bis(thiourea) Derivatives. *Cryst. Growth Des.* **2005**, *5*, 2288−2298.
(84) Custelcean, R. Crystal engineering with urea and thiourea hydrogen-bonding groups. *Chem. Commun.* **2008**, 295−307.
(85) Wagner, J. P.; Schreiner, P. R. London Dispersion in Molecular Chemistry—Reconsidering Steric Effects. *Angew. Chem., Int. Ed.* **2015**, *54*, 12274−12296.
(86) Liptrot, D. A.; Power, P. P. London dispersion forces in sterically crowded inorganic and organometallic molecules. *Nat. Rev. Chem.* **2017**, *1*, 0004.
(87) Mitoraj, M. P.; Sagan, F.; Szczepanik, D. W.; de Lange, J. H.; Ptaszek, A. L.; van Niekerk, D. M. E.; Cukrowski, I. Origin of Hydrocarbons Stability from a Computational Perspective: A Case Study of Ortho-Xylene Isomers. *ChemPhysChem* **2020**, *21*, 494−502.
(88) Cukrowski, I.; Sagan, F.; Mitoraj, M. P. On the Stability of Cis- and Trans-2-Butene Isomers. An Insight Based on the FAMSEC, IQA, and ETS-NOCV Schemes. *J. Comput. Chem.* **2016**, *37*, 2783−2798.
(89) Radi, S.; Toubi, Y.; Bacquet, M.; Degoutin, S.; Mabkhot, Y. N.; Garcia, Y. An inorganic−organic hybrid material made of a silica-immobilized Schiff base receptor and its preliminary use in heavy metal removal. *RSC Adv.* **2016**, *6*, 34212−34218.
(90) Sheldrick, G. M. *SHELXS-97 and SHELXL-97, Program for Crystal Structure Refinement*; University of Gottingen: Germany. 1997.
(91) Sheldrick, G. M. *Acta Crystallogr., Sect. A: Found. Crystallogr.* **2008**, *A64*, 112.
(92) Kresse, G.; Furthmüller, J. Efficiency of ab-initio total energy calculations for metals and semiconductors using a plane-wave basis set. *Comput. Mater. Sci.* **1996**, *6*, 15−50.
(93) Perdew, J. P.; Burke, K.; Ernzerhof, M. Generalized Gradient Approximation Made Simple. *Phys. Rev. Lett.* **1996**, *77*, 3865−3868.
(94) Grimme, S.; Antony, J.; Ehrlich, S.; Krieg, H. A consistent and accurate ab initio parametrization of density functional dispersion correction (DFT-D) for the 94 elements H-Pu. *J. Chem. Phys.* **2010**, *132*, 154104.
(95) *ADF2016, SCM, Theoretical Chemistry*; Vrije Universiteit: Amsterdam, The Netherlands, http://www.scm.com.
(96) te Velde, G.; Bickelhaupt, F. M.; Baerends, E. J.; Fonseca Guerra, C.; van Gisbergen, S. J. A.; Snijders, J. G.; Ziegler, T. , Chemistry with ADF. *J. Comput. Chem.* **2001**, *22*, 931−967.

https://doi.org/10.1021/acs.cgd.1c00352
Cryst. Growth Des. 2021, 21, 3562−3581